AD A036665

R-2057/1-PR
November 1976

Image Correlation: Part I Simulation and Analysis

H. H. Bailey, F. W. Blackwell, C. L. Lowery, J. A. Ratkovic

A report prepared for

UNITED STATES AIR FORCE PROJECT RAND

DISTRIBUTION STATEMENT
Approved for public release;
Distribution Unlimited

DDC
RECEIVED
MAR 8 1977

Rand
SANTA MONICA, CA. 90406

Statement A relevant to classified references on pg. 53. Document should remain as "A" ~~per~~ Jean Johnson, HQ USAF (RDQLR)

JEC
3/10/77

The research described in this report was sponsored by the United States Air Force under Contract No. F49620-77-C-0023 -- Monitored by the Directorate of Planning, Programming and Analysis, Deputy Chief of Staff, Research and Development, Hq USAF.

Reports of The Rand Corporation do not necessarily reflect the opinions or policies of the sponsors of Rand research.

R-2057/1-PR
November 1976

Image Correlation: Part I Simulation and Analysis

H. H. Bailey, F. W. Blackwell, C. L. Lowery, J. A. Ratkovic

A report prepared for

UNITED STATES AIR FORCE PROJECT RAND

APPROVED FOR PUBLIC RELEASE; DISTRIBUTION UNLIMITED

PRECEDING PAGE BLANK-NOT FILMED

PREFACE

This is the first part of a two-part report that describes research initiated at Rand in mid-1975 under the Project RAND research project "Target Acquisition." The subject is "map matching" or image correlation to achieve autonomous target acquisition and terminal guidance for missiles (both strategic and tactical), with particular emphasis on the acquisition phase.

Part I presents an analysis of the probabilities of correct and false acquisitions, extends it to include the effects of a number of common error sources, and describes computer simulations based on data samples from real scenes. Part II* provides a more general and more rigorous analytical approach. Some of the conclusions derive jointly from both phases of the study, but Part II is published separately because it is addressed to readers with a theoretical and mathematical interest in the subject.

Both reports should be of interest to defense and industrial project managers and engineers involved in the development of missile guidance, particularly those concerned with current or future correlator programs.

---

*H. W. Wessely, *Image Correlation, Part II: Theoretical Basis*, The Rand Corporation, R-2057/2-PR, November 1976.

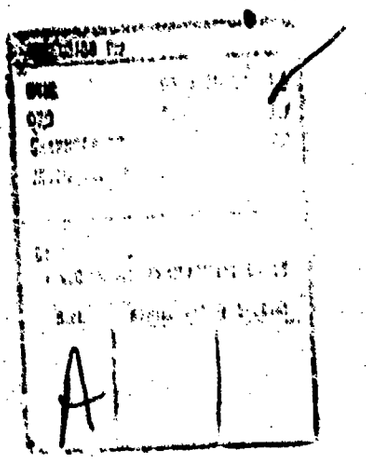

PRECEDING PAGE BLANK-NOT FILMED

SUMMARY

Image correlation or "map matching" makes possible a type of weapon guidance that provides autonomous target acquisition and tracking. This study analyzes the image correlation process, both theoretically and by using computerized simulations; primary emphasis is on the often neglected but crucial acquisition phase. (The requirement for achieving adequate terminal tracking accuracy in weapon delivery has been and is being studied extensively elsewhere and, for this report, is considered to be of secondary importance; it is simply assumed that, if necessary, operational systems could accommodate a software change to maximize tracking accuracy *after* the initial acquisition has been accomplished.)

The essential step in image correlation guidance is to find the position of "best fit" between two similar but nonidentical images or "maps": a *sensor* image of the terrain surrounding a desired target, obtained in real time as the weapon approaches, and a previously prepared *reference* image of roughly the same area. The match point is found by systematically displacing one map relative to the other and computing, for each of the many possible displacements, the value of a comparison function or "metric" that, ideally, has an extremum (max or min) value at the match point. The particular displacement, suitably scaled, that produces the extremum becomes the correction signal for the guidance system.

Unfortunately, precisely because the two maps are not identical--owing to detector noise, real changes in the scene, geometrical distortions, and several other causes that are discussed in this report--the displacement that produces the extremum does not *always* correspond to the correct match point. It only does so *on the average*. Accordingly, this analysis focuses on two topics of principal concern: (a) the probability of achieving a correct match (conversely, the probability of a "false lock" or, in military terms, a gross error) and (b) the selection of an appropriate comparison metric to maximize (a).

The probability of achieving a correct match, P_c, can be analyzed in a straightforward manner if one is willing to make several simplifying

but unrealistic assumptions. The unrealism comes in attempting to describe terrain--particularly terrain that has been modified by man--using only Gaussian statistics. The results of such an analysis are qualitatively correct, but quantitatively they tend to be pessimistic (as our analysis shows). Nevertheless, we use this approach in the first portion of this report, followed by a description of some simulations using real scene data. In Part II,* a broader perspective on the map-matching problem is undertaken and some important insights are derived.

In the simple Gaussian approach developed in Section II, two commonly used comparison metrics are calculated by using the so-called Product (a sum of products that is related to classical correlation) and MAD (mean absolute difference) algorithms, respectively. It is shown that in all cases P_c increases with the size of the data sample and with the elemental signal-to-noise ratio (S/N), and decreases (slowly) with increasing search area. It is also shown that at low S/N, the Product algorithm is the preferred one (i.e., it leads to higher probabilities of correct lock), but at high S/N the MAD algorithm is preferred.

In Section III, the same methods are extended to include the effects of a number of commonly encountered systematic error sources. Geometrical errors include synchronization (an effect peculiar to digital systems in which the picture elements of the two maps are staggered by some unknown fraction of a picture element), rotation, and scale factor (magnification). These all have the effect of reducing the peak value of P_c and increasing the width of that function; i.e., they both increase the chances of a false lock and decrease the tracking accuracy. If rotation and scale are controlled, as they usually can be in practice, such that $n\theta \leq 1$ and $n(\rho - 1) \leq 1$, then performance is not seriously degraded. Here n is the number of independent samples across the (smaller) sensor map, θ is the rotation in radians, and ρ is the magnification. The synchronization error, however, is inherently uncontrollable and, in the

*R-2057/2-PR, *Image Correlation, Part II: Theoretical Basis* (see Ref. 1).

case of uncorrelated data, can have roughly the same effect as reducing any S/N to less than unity. Several kinds of systematic intensity errors can also occur in practice. Generally these primarily affect the peak value of P_c. A simple uniform reduction in signal level (due to an erroneous gain setting, for example) is shown to be quite serious for the MAD algorithm, but the Product algorithm is unaffected. Other and more complex intensity errors are treated in Section IV. The principal conclusion is that real systems suffer from a number of errors that, loosely speaking, lower the effective value of S/N, so that the higher values which, according to Section II, would render the MAD or similar algorithms attractive are seldom realized in practice.

Some tests of the foregoing theory are described in Section IV. These tests were carried out by means of computer simulations of the map-matching process using some digitized samples of data taken from real scenes. Four scenes, differing in both visual "texture" and autocorrelation length, were selected out of a large available data base to represent different types of terrain. They are crudely categorized as agricultural, mountain, desert, and suburban. The most extensive simulations involved adding Gaussian noise to patches lifted out of each scene, and then comparing the so-modified "sensor" map with the original or "reference" map, using both the Product and the MAD metrics. Both algorithms consistently performed significantly better (i.e., had higher P_c) when operating on these real data than was predicted by the theory developed in Section II. This phenomenon is probably due to the fact that (a) the scenes are non-Gaussian, whereas the theory specifically postulated Gaussian statistics, and (b) the very features and structure that modify the statistics render the scenes "more unique," with properties that the comparison metrics are able to exploit.

Simulations were also carried out with synchronization, scale factor, rotation, and "gain" errors introduced on the same samples of real scene data; these results were consistent with the theory. In addition, a few experiments were conducted in which substantial blocks of the sensor scene were altered drastically to simulate the effects of shadows and jamming. The Product algorithm is more resistant to "shadows" than the MAD algorithm, as expected; but both are seriously degraded by large

amounts of high-intensity "jamming." Finally, a small number of gray-level quantization codes were tried. In these tests, P_c increased monotonically with the number of levels used, but 8-level (3-bit) codes were about 90 percent as good as "continuous" (e.g., 64-level) codes and so should suffice for many applications.

The fundamental nature of the map-matching problem is reexamined in Part II of this study, where the degree of theoretical justification for the use of the various comparison metrics is also investigated. Since the problem is basically one in statistical decision theory, the analysis of Part II shows that the optimum solution is achieved by computing the likelihood ratio for each comparison and then choosing the match point at the place where the likelihood ratio is maximum. Unfortunately, that computation requires a knowledge of the N-dimensional joint probability distributions--functions that are unknown and, in a practical sense, unmeasurable. Hence, one must resort to approximations. These usually take the form of maximizing or minimizing one of several functions, herein called "metrics." In much current work, these are chosen almost arbitrarily and therefore must be subjected to essentially experimental validation. By considering two-picture-element scenes, such that the likelihood ratio and several of the commonly used metrics can be expressed in simple algebraic form and discussed in geometrical terms, the essential features of the various metrics are explained and compared with the likelihood ratio. In this way heuristic arguments are developed that support the use of the Product algorithm when S/N is low and the MAD algorithm when S/N is high.

Two major conclusions were derived from this study and are presented in Section V. The principal conclusion is that by using the methods illustrated in this report, an approximate lower bound on the value of P_c can be calculated, so that one can, at least in principle, design systems to an acquisition specification. Several quantitative relationships between P_c and various system parameters have been derived and largely confirmed by simulation testing. These can be used to carry out a number of design tradeoffs, including a balancing of the costs of a tighter overall P_c requirement with the loss of those weapons that fail to acquire. The theoretical model of the random Gaussian scene

is known to be not completely realistic, but it appears to err on the conservative side. Thus a "floor" for P_c can be established, which should permit the flight test performance of future properly designed systems to be somewhat better (i.e., to exhibit fewer gross errors) than is predicted by this theory.

The second conclusion is that there ought to be better algorithms than those that have usually been used in the past. Since (a) there is at present little theoretical basis for the commonly used comparison metrics, and (b) most real terrain contains features beyond those describable by simple Gaussian statistics, it seems both reasonable and not inconsistent with theory to search for more efficient ways to carry out the initial map-matching or target-acquisition function. In particular, drastic preprocessing to extract special features of a given scene, using techniques currently being developed and exploited in the field of pattern recognition, appears promising for the generation of more efficient algorithms. Steps that can be taken in this direction are briefly outlined.

ACKNOWLEDGMENTS

The authors gratefully acknowledge the assistance given by their colleagues, H. W. Wessely and W. Sollfrey. Wessely provided valuable consultation throughout the study and assisted materially in the preparation of the report. Sollfrey made a number of specific calculations and gave the report a careful and insightful technical review.

PRECEDING PAGE BLANK-NOT FILMED

CONTENTS

PRECEDING PAGE BLANK-NOT FILMED

FIGURES

PRECEDING PAGE BLANK-NOT FILMED

TABLES

I. INTRODUCTION

The military problem that initiated this study, and to which the results are relevant, is one of achieving autonomous target acquisition and tracking for indirectly fired weapons. Such weapons will be required in the future when manned aircraft are unable to penetrate to within visual line-of-sight to intended targets without suffering intolerable losses. The acquisition function is the more difficult of the two, so much so that to date only in exceptional instances is human intervention not required at some stage of that process, whereas automatic tracking following acquisition or "lock-on" is commonplace. Both requirements--that for target acquisition after weapon launch from standoff and that for accurate terminal guidance--dictate (with few exceptions) the presence of some kind of two-dimensional imaging sensor on board the weapon.

The most common approach to in-flight acquisition is to acquire the target in "real time" with direct human assistance, using radio links between the weapon and its launch aircraft (or via relays to some other control point). Radio links enable a human observer to find, identify, and "acquire" the target, and incidentally also to monitor the subsequent tracking operation and refine it as needed. This approach has its obvious costs and vulnerabilities. Alternatively, if prior reconnaissance imagery of the target area is available, an observer can study it, find the target, and mark it. If this marked imagery (in some appropriate form) is then placed on board the weapon, together with the sensor for obtaining "live" imagery, all that is required in real time is to bring these two images into coincidence. This process can be mechanized on the weapon. At that point, the weapon will "know" where it is with respect to the target and will be able to steer itself to impact. This approach, too, has its costs and vulnerabilities--both quite different from the data-link approach. This type of autonomous acquisition and tracking system is the subject of the present study.

The technical problem that needs to be examined reduces to one of comparing two pieces of terrain imagery that are similar, but certainly not identical, and that are presumably at least partially overlapping. The acquisition function reduces to answering, with some preassigned level of confidence, the question "Do the two images in fact overlap, so that they can be brought into registry?" The tracking function corresponds to measuring, as accurately as possible, the displacement between the centers of the two images after registration has been achieved, and repeating this measurement with updated sensor images obtained as the weapon approaches the target. These displacements are then supplied to the guidance system to effect terminal guidance and "homing" onto the target. The image registration process is colloquially referred to as "map matching," or sometimes as image correlation--although correlation in the strict mathematical definition of that word may or may not be required.

The idea of using map-matching techniques for missile guidance has been around for a long time, and indeed the Air Force has actively sponsored hardware development programs in this field for at least 20 years. The implementations in early systems were all analog--either optomechanical or electro-optical in nature; today, in keeping with current integrated circuit technology, most of the work is digital. However, the principles, and the fundamental strengths and weaknesses, are still the same. The major weakness of these systems, and the reason for more failures than successes in the past, is that they are inherently susceptible to false matches, which, of course, leads to gross errors and wasted (or worse) weapons. In fact, past systems that have had the greatest, though still marginal, level of success were those that minimized the acquisition requirement--either by more or less continuously tracking a succession of planned checkpoint areas all the way from launch or, in the case of manned bombers, by using a crew member to monitor the acquisition phase and relying on the correlator only for accurate tracking. Past analyses [2] of correlation guidance systems have also concentrated on the achievable tracking accuracy and, with one notable exception [3], have almost ignored the "false-lock" or

gross-error problem. Because of this unfortunate history in an otherwise promising and needed area of development, the principal effort in the current study has been directed to more fully understanding the acquisition aspects of image correlation.

II. A PRELIMINARY ANALYTICAL APPROACH

STATEMENT OF THE PROBLEM

The mathematical formulation of the correlation problem can be introduced as follows. Although images have an inherently two-dimensional* format, initially it will suffice (and it will simplify the exposition) to use but a single index to designate the picture elements in a map or scene. The implied extension to a full two-dimensional notation is straightforward and should cause no confusion or loss of generality, at least in concept.

The operational situation to be modeled is the following: An airborne or satellite-borne sensor images a scene on the ground containing a target. This image is broken down into an array of M (square) picture elements (sometimes called pixels), and a value X_I, representing a certain level of a gray scale, is assigned to each element. These data are stored in a computer memory and are henceforth referred to as the "reference map." This reference map, shown schematically in Fig. 1, contains the target located at the center. At some time later, another sensor on board an aircraft or a weapon images a smaller portion of this same scene containing N elements, Y_I, which are similarly digitized to form a "sensor map." (In Fig. 1, both maps are assumed to be square, purely for convenience of notation; thus, $m = \sqrt{M}$ and $n = \sqrt{N}$ represent the number of picture elements in one row of the reference and sensor maps, respectively.) The center of the sensor map, which is related to the boresight of the weapon, will generally be displaced from the center of the reference map by some unknown amount that depends on midcourse navigation and pointing errors, and the sensor map may or may not actually contain the target. The first problem, then, is to find (if it exists) the portion of the reference map that matches the sensor map. Once this is accomplished, the displacement or offset between the centers of the two maps (shown with two components [K,L] in Fig. 1) serves as the correction signal to the guidance/control subsystem.

---

*Three-dimensional images and 3-D terrain/structure modeling are, of course, possible, but these are ignored for the present.

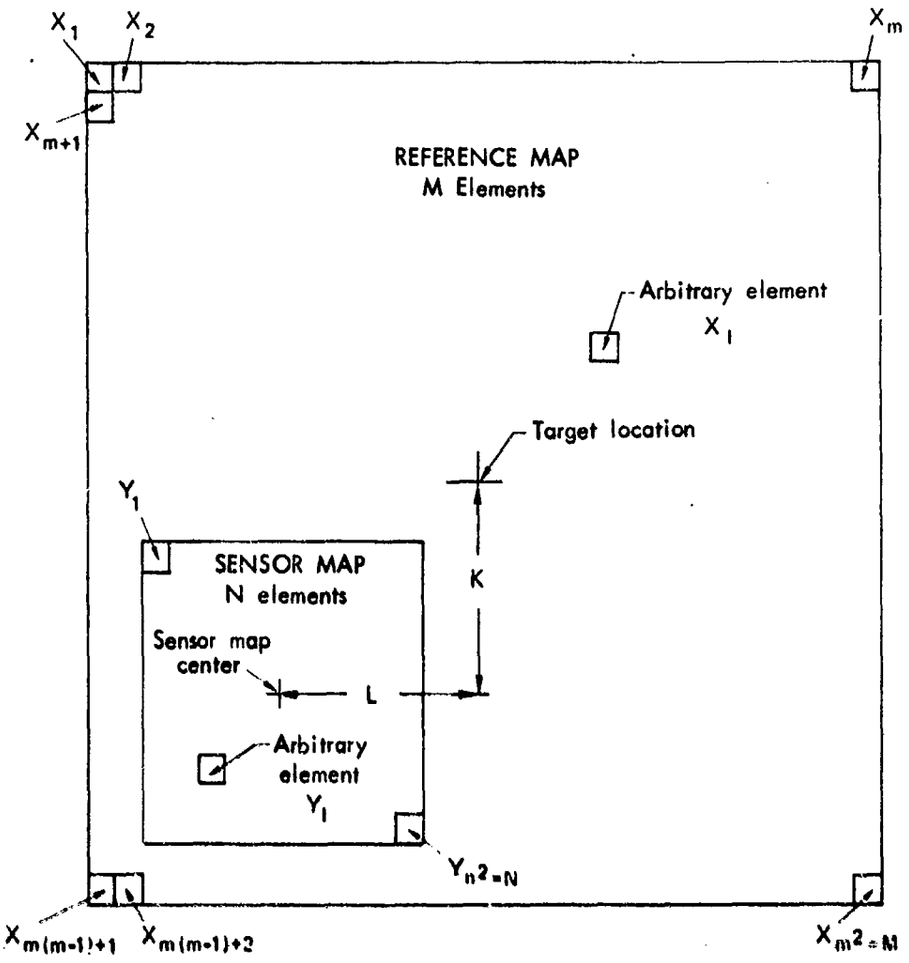

Fig. 1 — Map definitions

To simplify the exposition, it has been explicitly assumed above that the sensor map is smaller than the reference map. In principle, it could be the other way around: a small reference map could be matched against a large sensor map, and any analysis of one case would be completely applicable to the other by simply interchanging the definitions of M and N (M always being the larger). The differences are, of course, important for hardware implementation choices that may be driven by economic and/or dynamic considerations. For example, applications involving only navigational position-fixing en route would probably not warrant the cost of extensive reference preparation and onboard storage, so that the second alternative (using a small reference)

might be preferred. However, in the case of terminal homing against known targets, the time constraint on acquiring data for the last steering correction, combined with the added cost of a large field-of-view sensor, would argue the other way. Since the primary concern of this report is with terminal homing, the use of a small sensor map and a large reference map is assumed consistently; but, to repeat, the analysis really covers both cases.

In attempting to properly locate the sensor map relative to the reference map, the sensor map must be compared with numerous equally sized portions of the reference map. In Fig. 2, the sensor map is shown in two positions--one is the correct or matching position, and

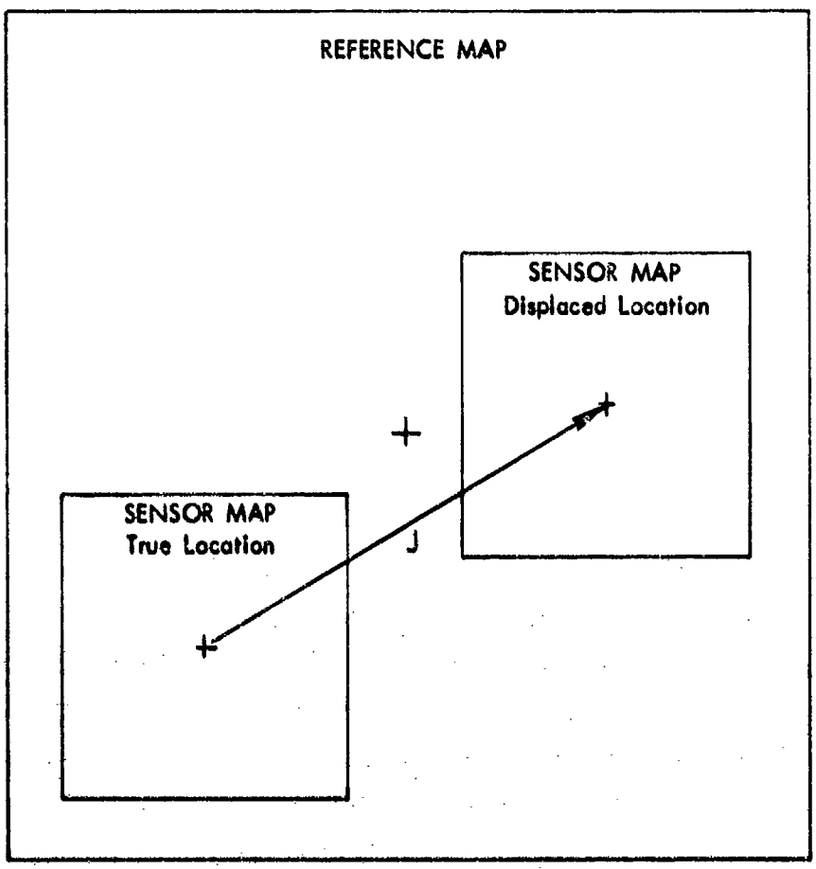

Fig. 2—Definition of map displacement

the other is one of the Q possible nonmatching positions.* The displacement from the correct location of the sensor map to any arbitrary position is defined to be the displacement vector, here indicated by a single index, J. In the absence of certain geometrical errors to be discussed later, all elements of the sensor map are correctly positioned with the corresponding elements of the reference map when the displacement vector is zero. The acquisition phase of the image correlation problem thus reduces to a two-state discrimination problem, i.e., to one of discriminating between the case when the displacement vector equals zero (termed the in-register case) and the case when it does not (termed the out-of-register case).

"METRICS" AND FORMULAS FOR P_c

The actual point-by-point comparison of the sensor map with the reference map is made by computing the value of one of several possible functions of the displacement, J. Algorithms suitable for this computation can be considered, for the moment, as arbitrarily selected functions or "metrics" whose efficacy is to be tested empirically. The justification (or lack of it) for some of the possible choices is discussed more carefully in Part II of this report [1]. The most commonly used algorithm is derived from classical correlation, which is approximated by computing finite sums, sometimes normalized, of the form

$$\phi_1(J) = \frac{1}{N} \sum_{I=1}^{N} X_{I+J} Y_I \quad \text{(Prod)} . \tag{1}$$

This is referred to as the Product algorithm. The next most important metric is the mean absolute difference (MAD) algorithm, defined as

$$\phi_2(J) = \frac{1}{N} \sum_{I=1}^{N} |X_{I+J} - Y_I| \quad \text{(MAD)} . \tag{2}$$

*When the separation between positions is measured in units of the cell size, this number Q is, in the case of one-dimensional strip maps, simply M - N; for two-dimensional maps, it is $(m - n + 1)^2 - 1$.

A third function, the difference squared,

$$\phi_3(J) = \frac{1}{N} \sum_{I=1}^{N} (X_{I+J} - Y_I)^2 ,$$

is of some theoretical interest and is mentioned again in Part II; however, over the range of parameter values explored here, this function always gives lower values for the probability of correct lock than does ϕ_2. Many other algorithms have been tried, by us and by others [4], with the same general conclusion. The exposition here is confined to the Product and MAD algorithms as being representative of the two principal classes of algorithms that have been proposed to date.

When the maps are in register, J = 0; and if no errors are present, $X_I = Y_I$. It can easily be shown that $\phi_1(J)$ has a maximum value and that $\phi_2(J)$ has a minimum value under these conditions. Thus, if it can be assumed that for some test position the two maps really do coincide, then the value of J for which $\phi(J)$ is an extremum essentially defines the best match position between the two maps. However, in the presence of noise and various other errors to be discussed, the extremum only defines the correct match point *on the average*. Because of these effects there is only a certain probability, P_c (over an infinite ensemble of maps), that the extremum actually defines the correct match point. If $p(\phi|S)$ denotes the conditional probability density of the value of the metric when the maps are matched (S = signal present), and if $p(\phi|B)$ denotes the conditional probability density of the value of the metric when the maps are mismatched (B = background present), then for a maximizing metric the probability of correct acquisition is given by

$$P_c = \int_{-\infty}^{\infty} p(\phi|S) \left[\int_{-\infty}^{\phi} p(\phi'|B)\, d\phi' \right]^Q d\phi , \qquad (3)$$

where Q, as before, denotes the number of mismatched positions. A simple change in the limits of integration describes the probability

of correct acquisition for a minimizing metric. $1 - P_c$, of course, gives the probability of a false lock or gross error--the problem mentioned in Section I.

One straightforward, though certainly only approximate, method of calculating P_c has been proposed by Johnson [5]. His method is approximate because of the large number of quite fundamental assumptions he has made in order to render the analysis tractable. Some of these assumptions are known to be invalid, at least some of the time, if not always. Nevertheless, calculations carried out using his method can provide a good deal of insight into the operation of correlators. Johnson's method, with certain extensions described below, provides the basis for much of the work discussed in this report. His assumptions can be stated as follows:

1. The sensor signal (albeit distorted) does exist in the reference data--an assumption that is not made in the broader Bayesian approach discussed in Part II of this study.
2. The reference data, X_I, are assumed to be stationary, ergodic, and Gaussian distributed with zero mean* and variance σ_x^2. (Typical real scenes contain a two-dimensional structure, usually but not necessarily man made--field boundaries, roads, buildings--that are clearly non-Gaussian.)
3. The sensor data, Y_I, are assumed to be the reference data corrupted by noise, such that $Y_I = X_I + N_I$, with N_I stationary, ergodic, and Gaussian distributed with zero mean and variance σ_n^2. (Thus, only additive, white, uncorrelated noise is considered at this point. Other differences between X_I and Y_I are discussed later.) The ratio σ_x^2/σ_n^2 is designated S/N and is referred to as the signal-to-noise ratio.
4. The reference map values, X_I, the sensor map values, Y_I, and the noise values, N_I, are separately and mutually statistically independent random variables. (This is probably not

*Data with a nonzero mean can easily be reduced to meet this condition by suitable preprocessing.

a "serious" or poorly met assumption; it does require, however, that when a scene exhibits spatial correlation, M and N must be interpreted as the numbers of independent data samples in the reference and sensor maps, respectively.)

5. The distribution of the values of the metric over the ensemble of maps is also Gaussian. (The error introduced by this demonstrably false assumption may be small as long as the number of elements in the sensor map is large enough for the central limit theorem to hold. This point has been investigated in detail by Sollfrey,* but only for the Product algorithm; he finds that, due to some compensating effects, the correct result is not seriously different from the Gaussian calculation.)

With these assumptions, it is indeed straightforward, though somewhat tedious, to calculate the ensemble means and variances of various metrics both for in-register (J = 0) and out-of-register (J ≠ 0) conditions, and then to compute P_c by means of a formula of the form

$$P_c = \frac{1}{\sqrt{2\pi}\,\sigma_o} \int_{-\infty}^{+\infty} \exp\left[\frac{-w^2}{2\sigma_o^2}\right] \cdot \left[\frac{1}{2} \pm \frac{1}{2}\,\mathrm{erf}\,\frac{(\bar{\phi}_o - \bar{\phi}_j) + w}{\sqrt{2}\,\sigma_j}\right]^Q dw \,, \quad (4)$$

where $\bar{\phi}_o$ and $\bar{\phi}_j$ are the ensemble mean values of the metric when the maps are in and out of register, respectively; σ_o^2 and σ_j^2 are the ensemble variances when the maps are in and out of register; w is $\phi_o - \bar{\phi}_o$; and Q is the number of out-of-register values of J as defined in the footnote on p. 7. The quantities $\bar{\phi}_o$, σ_o^2, and σ_j^2 are simply related† to N, σ_x^2, and σ_n^2. Values of P_c have been obtained by numerical integration of Eq. (4) for various values of the parameters N, Q, and S/N

*W. Sollfrey, The Rand Corporation (private communication).

†The relevant ensemble statistics for the quantities $\bar{\phi}_o$, σ_o^2, and σ_j^2 are shown in the table below. Corresponding formulas for other

within the ranges of $10 \leq N \leq 10^4$, $10 \leq Q \leq 10^6$, and $0.1 \leq S/N \leq 30$, using Rand's IBM 370/158 computer.

NUMERICAL RESULTS

Some of the results of these calculations are shown in Fig. 3, where P_c is plotted as a function of the S/N ratio for two specific values of N and Q, for both the Product and MAD algorithms. In order to illustrate more clearly the nature of the dependence on the parameters N and Q, additional data are presented in Figs. 4 through 6 in the form of contours of constant probability (P_c = 0.99, 0.90, 0.70, and 0.50)* as a function of N and Q for three different values of S/N, again for both algorithms.

CONCLUSIONS

The following significant conclusions† can be drawn from these data.

- The probability of correct match, P_c, increases with an increase in the elemental signal-to-noise ratio, S/N, and with an increase in the size of the data sample, N. (This, of course, is to be expected, since the *total* signal-to-noise ratio represented by the sum of the contribution from each sensor map element is increased by either an increase in the elemental signal-to-noise ratio or an increase in the total number of sensor map elements.)

algorithms have been derived but are not needed here.

Algorithm	$\bar{\Phi}_0$	σ_0^2	σ_j^2
Prod	σ_x^2	$(\sigma_x^2/N)(2\sigma_x^2 + \sigma_n^2)$	$(\sigma_x^2/N)(\sigma_x^2 + \sigma_n^2)$
MAD	$\sqrt{2/\pi}\,\sigma_n$	$(1 - 2/\pi)(\sigma_x^2/N)$	$(1 - 2/\pi)(\sigma_x^2 + \sigma_n^2)/N$

*Values of P_c as low as 0.7 and 0.5 would probably be unsatisfactory for military systems; however, they are plotted in order to show trends and to permit extrapolations and interpolations to be made.

†Similar conclusions have been reached by Lockheed [4] in a systematic survey of many possible algorithms; however, their principal criterion for judging the success of algorithms was the accuracy of the position measurement, whereas ours is the probability of correct match.

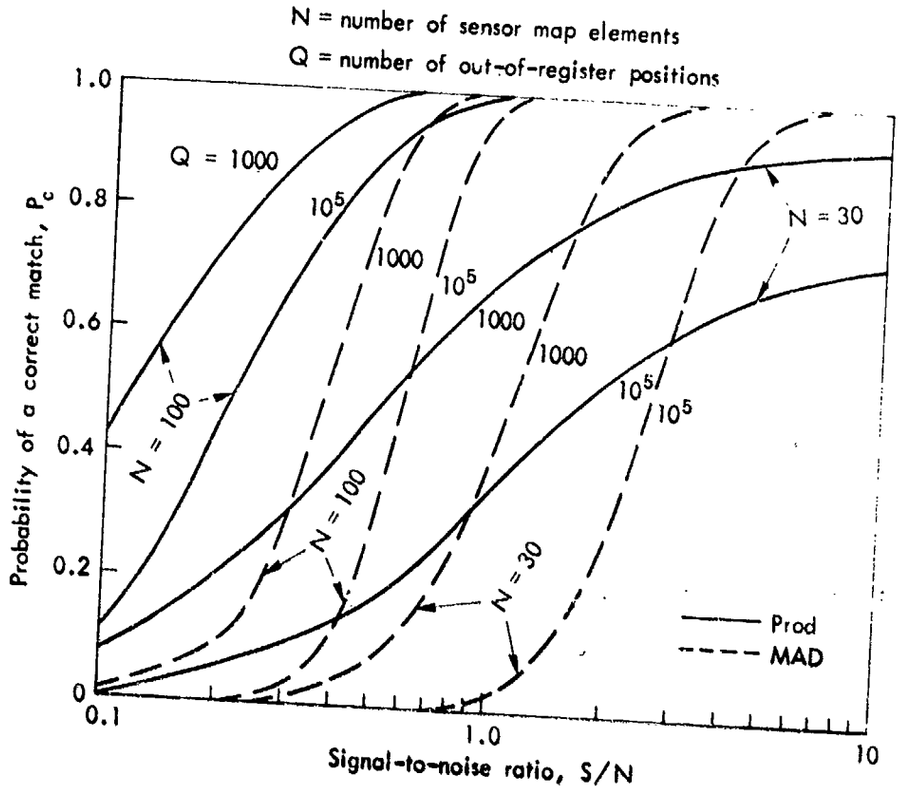

Fig. 3—P_c versus S/N for additive noise only

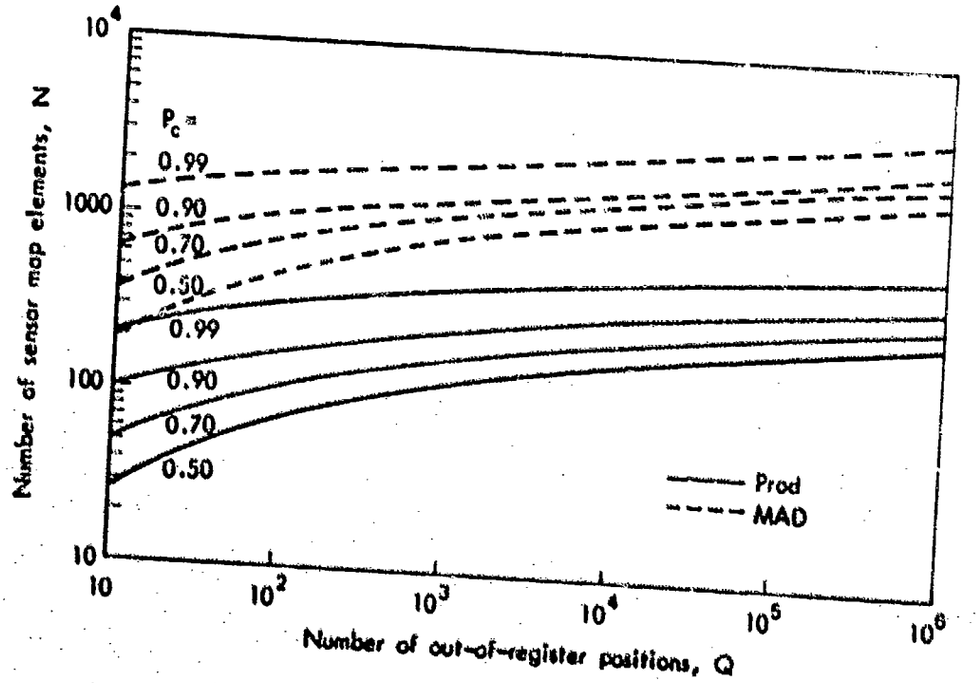

Fig. 4—Probability contours for S/N = 0.1

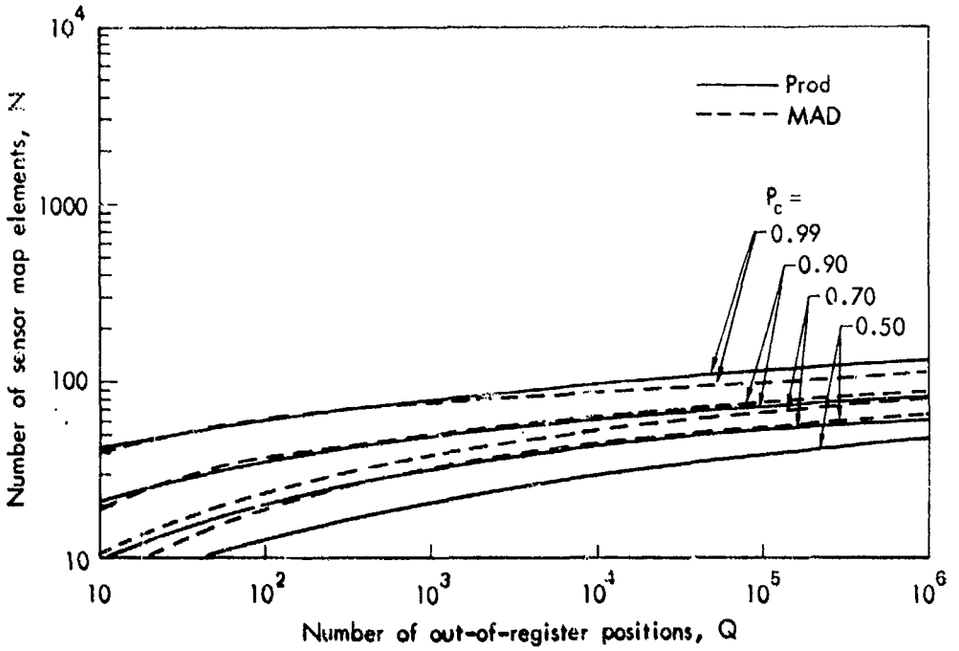

Fig. 5—Probability contours for S/N = 1.0

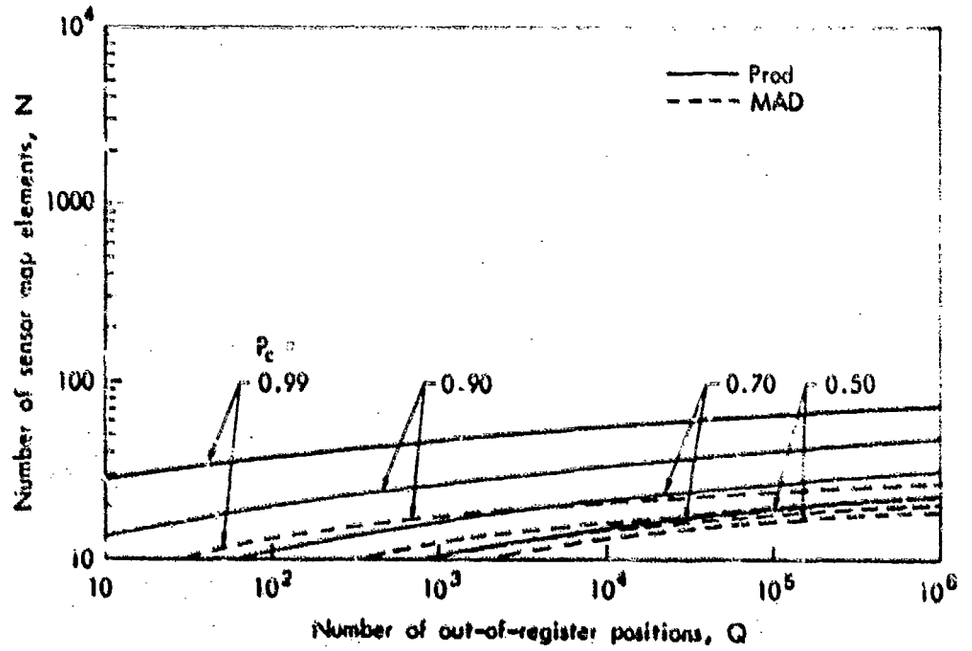

Fig. 6—Probability contours for S/N = 30

- The probability of correct match, P_c, decreases with increasing Q, the number of out-of-register positions, but the decrease with increasing Q is relatively weak in comparison to the effect of a change in the number of sensor map elements, N, as shown in Figs. 4 through 6. (This behavior can be explained qualitatively by the fact that an increase in the number of out-of-register positions tends to increase the root-mean-square variation in the value of the metric roughly as the square root of Q, whereas an increase in N increases the value of the metric linearly when the two maps are matched.)

- At low signal-to-noise ratios ($S/N \leq 1$), the Product is the better algorithm, i.e., it leads to higher values of P_c. (This result is analogous to the well-known finding in statistical communication theory that a correlation receiver is the "matched filter," the best receiver for detecting a signal in noise; however, as explained in Part II of this report, the map-matching problem is fundamentally different and the apparent analogy cannot be pressed.)

- At high signal-to-noise ratios ($S/N \geq 3$), the MAD is the better algorithm.* (A heuristic explanation for this result is also given in Part II. More importantly, it is shown next in Section III that, in real-world systems applications, the high values of S/N that would justify use of the MAD metric are very seldom realized.)

---

*When $1 < S/N > 3$, results are mixed and the choice of algorithm is not critical.

III. TREATMENT OF VARIOUS SYSTEMATIC ERRORS

QUALITATIVE DISCUSSION OF ERROR SOURCES

The method described above can be extended to analyze, at least approximately, the effectiveness of correlation techniques for target acquisition when error sources other than simple additive noise are present. In general, there are at least four classes of systematic errors that can degrade correlation performance:

1. Geometrical distortions.
2. Systematic intensity changes.
3. Quantization errors.
4. Enemy jamming.

1. Any *geometrical distortion* of the sensor map coordinates relative to the reference map coordinates degrades, in ways that are discussed below, the performance of a map-matching system. The four most important types of geometrical distortion are synchronization, rotation scale factor (magnification), and perspective errors. The detailed analysis of these effects, for digital systems, involves synthesizing a grid of cells each of which is given a value that is an appropriately weighted average of the values of the distorted cells that partially overlap each of the undistorted cells. These errors are illustrated in Fig. 7, where, for each case, the four cells surrounding the center of the reference map are depicted, together with the corresponding cells of the distorted sensor map.

Synchronization errors occur because there is no way to ensure a common origin between the sensor and reference map grids. As shown in the figure, this type of error results in all the grid elements of one map being fractionally displaced from those of the other map. This displacement can cause each sensor map grid element to overlap as many as four grid elements of the reference map. The effects of synchronization errors are most significant when the dimensions of a grid element are comparable to the average dimensions of a statistically independent scene element.

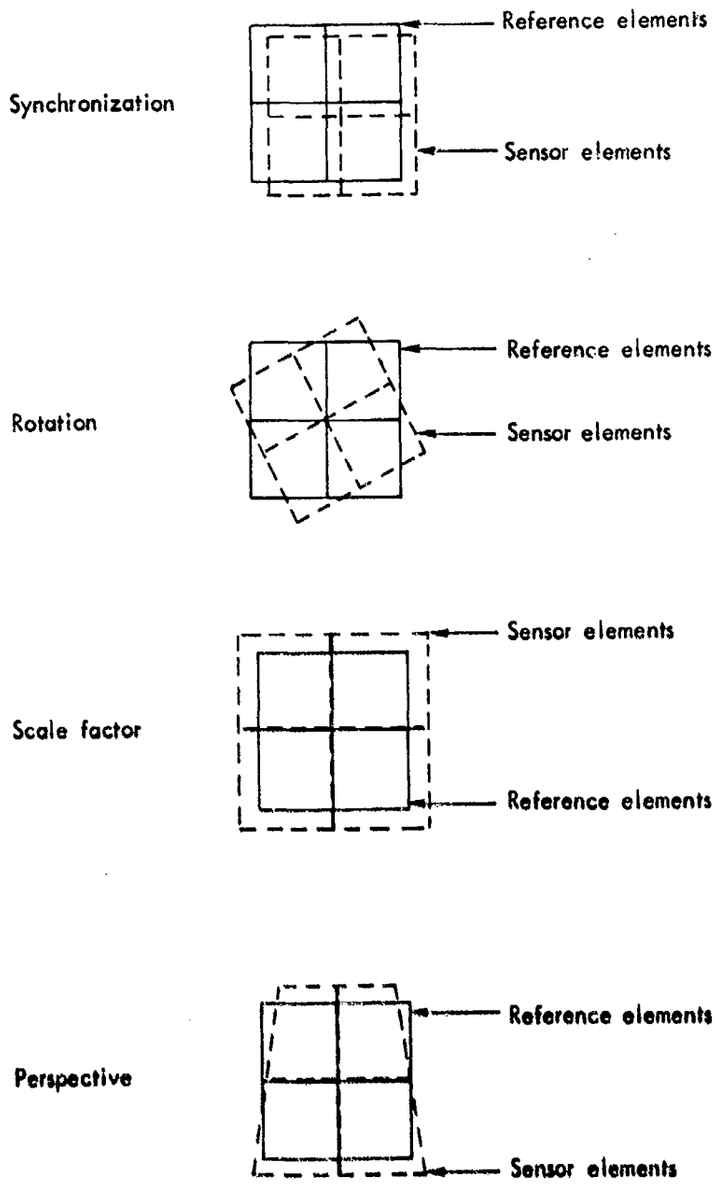

Fig. 7 — Geometrical distortion errors

Rotation errors can be caused by heading or attitude reference errors on board the weapon. If the sensor map is centered but rotated relative to the reference map, the map-matching process compares a single sensor cell with a combination of fractions of both matching and nonmatching reference cells. The amount of overlap with nonmatching cells increases as one moves radially outward from the center of the two maps.

Uniform magnification or scale errors are primarily caused by errors in weapon altitude or range to the target, although in some cases they may be caused by several other effects as well. In the presence of scale factor errors, the sensor elements are dimensioned either somewhat larger or somewhat smaller than the reference map elements. Consequently, elements of the sensor map, when overlaid on the reference scene, will again encompass both matching and nonmatching reference elements, with the amount of nonmatching overlap increasing as one moves radially outward from the center.

Perspective errors occur when the sensor views the reference area from a different position in space, because of midcourse navigation inaccuracies, for example. Owing to the difference in perspective, a grid pattern of square cells is transformed into an array of trapezoids. Thus, the effect is similar to a linearly varying scale factor error.

When geometrical distortions are present, only a partial match between sensor and reference map elements is possible. When the map centers are slightly displaced, some of the previously nonmatching map elements are brought into coincidence, so that a partial match condition holds for these displacements. The overall effects on the correlation function or comparison metric are thus twofold: the peak value of the metric for the matched condition is reduced, and the breadth of the function is increased.

2. *Systematic intensity errors* include all changes in the amplitude (or intensity) of the sensed scene relative to the reference scene that cannot be attributed to sensor noise. These changes can be aggregated into four general categories: (a) uniform change in overall signal level, (b) shadowing and obscurations, (c) changes in scene reflectivity/emissivity, and (d) reference map construction errors.

The overall signal level of the sensor scene relative to the reference scene can be altered by changes in scene illumination (e.g., day/night or sun/overcast) or by changes in sensor gain settings. Changes in the optical properties of the atmosphere can also change the overall signal level and/or the contrast perceived by the sensor. Shadows due to clouds or changes in sun angle, and obscurations due to intervening hills or foliage, cause blocks of sensor data elements to be totally dissimilar to the corresponding reference data elements. The reflectivity of certain portions of a scene can change drastically as a result of physical changes on the ground, such as snowfall or flooding, or less drastically but significantly as a result of differences in moisture content or seasonal changes in foliage and vegetation, or to a still lesser degree simply because of differences in the direction of the illumination by either active sensors or the sun at different times of day. Finally, the sensor scene can be different from the reference scene owing to actual changes in the reference scene (e.g., new man-made objects) and to reference map construction errors. This last category includes all errors made in producing the reference map, but primarily refers to errors made in transforming the original reconnaissance data taken in one spectral region (e.g., photographic) into a reference map for use with a "live" sensor in a different spectral region (such as infrared or millimeter waves).

These systematic errors generally do not increase the width of the correlation function significantly, but they do certainly reduce the differential between the in- and out-of-register values, thereby increasing the possibility for false locks.

3. In digital correlation systems, the sensor data, which are usually analog in nature originally and may have any one of a continuum of values at each pixel, are quantized into discrete levels and encoded. This process gives rise to what is sometimes called (through analogy with photographic systems) gray-level coding errors, or, more generally, *quantization errors*. The effects of quantization become important when only a few gray levels are used and when other errors are present simultaneously. Under those conditions, a signal that is distorted or has had noise added to it may either be coded exactly like

the original (in which case, the effect of the noise or distortion has been eliminated) or it may be coded at a different level (in which case the effect of the original error is usually exacerbated). Thus, the effect is something like the addition of noise, but it is a peculiar, non-Gaussian, kind of noise.

4. Finally, *enemy jamming* can cause (a) additional noise, possibly time varying, in all or a portion of the sensor elements or (b), in severe cases, complete saturation of most or all of the sensor elements. As with the "block" errors described above, the principal effect of jamming is usually to weaken the extremum value of the comparison metric, thus decreasing P_c.

ANALYSIS OF GEOMETRIC ERRORS

Of the geometric errors, synchronization, scale factor, and rotation errors have been examined explicitly. Because of the difficulty in modeling perspective errors, and because results generally similar to those produced by scale factor errors are to be expected, this type of geometric distortion has not been evaluated here. The analysis of the effects of uniform intensity errors are described here; the effects of quantization and a brief simulation of enemy jamming are reported in Section IV.

SYNCHRONIZATION

As mentioned previously, a synchronization error causes every element in the sensor map to be fractionally displaced, usually both vertically and horizontally, from the corresponding elements of the reference map. The amount of sensor/reference map overlap can be measured by the parameters α_i as shown in Fig. 8. Thus, a new reference map, X'_I, can be established by constructing a properly weighted average of the values in the four cells that partially overlap cell Y_{I+J}.

This procedure enables one to use Eq. (4) for calculating the acquisition probability in the presence of a specified synchronization error. The calculation involves two preliminary steps: (1) setting up the necessary statistical quantities, i.e., the ensemble means and variances of both in- and out-of-register comparison metrics (as above),

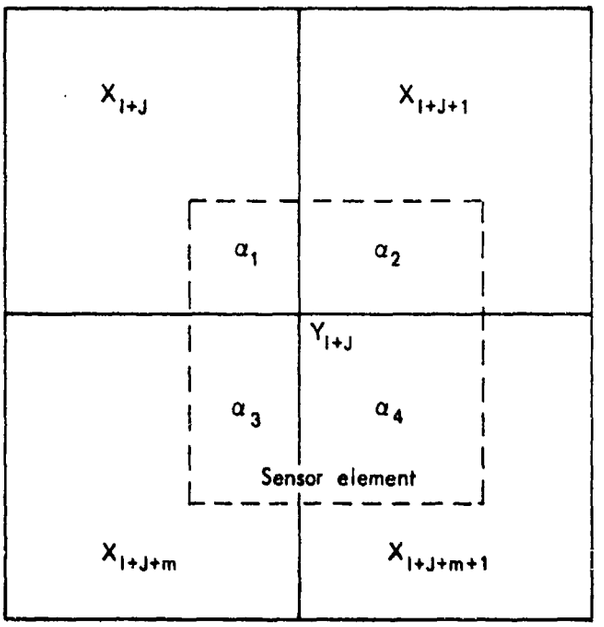

If α_1 = fractional area of cell X_{I+J} overlapping cell Y_{I+J}, etc.,
then $X'_{I+J} = \alpha_1 X_{I+J} + \alpha_2 X_{I+J+1} + \alpha_3 X_{I+J+m} + \alpha_4 X_{I+J+m+1}$.

Fig. 8—Cell construction for analysis of synchronization errors

and (2) finding the extremum of the four partially overlapping positions. Specifically, for this second step a new random variable is formed that is the maximum (minimum) of all in-partial-register values of the metric. The probability density function of this random variable can be expressed in terms of the probability density functions of the four in-partial-register metric values. Then, P_c can be calculated by replacing the distribution of the in-register correlation function (in the standard case of only one match point) with this distribution of the maximum value, and proceeding with the approach outlined previously.

Some of the results of this analysis are presented in Figs. 9 through 11 in the form (as before) of P_c contours. The worst-case synchronization error (producing the lowest values of P_c) occurs when each sensor element overlaps four reference elements and the areas of overlap are equal ($\alpha_1 = \alpha_2 = \alpha_3 = \alpha_4 = 0.25$). An examination of these contours shows the Product algorithm to be superior to the MAD algorithm

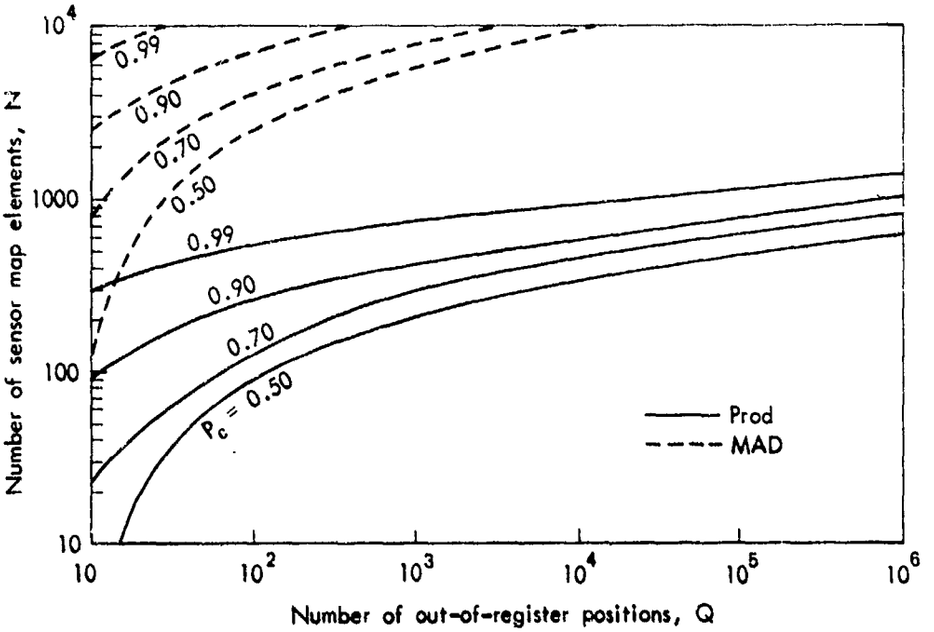

Fig. 9—Probability contours for S/N = 0.1 + maximum synchronization error

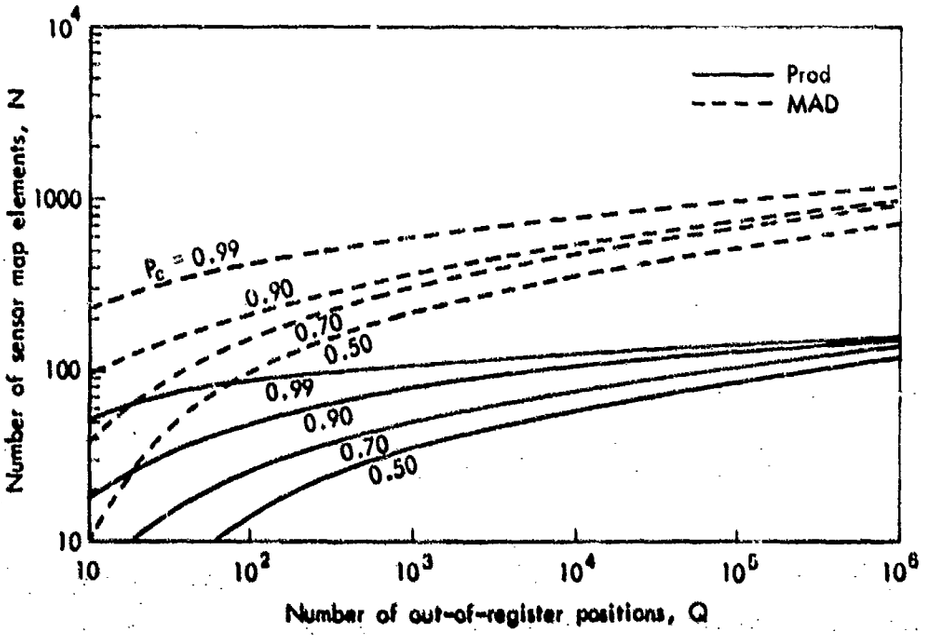

Fig. 10—Probability contours for S/N = 1.0 + maximum synchronization error

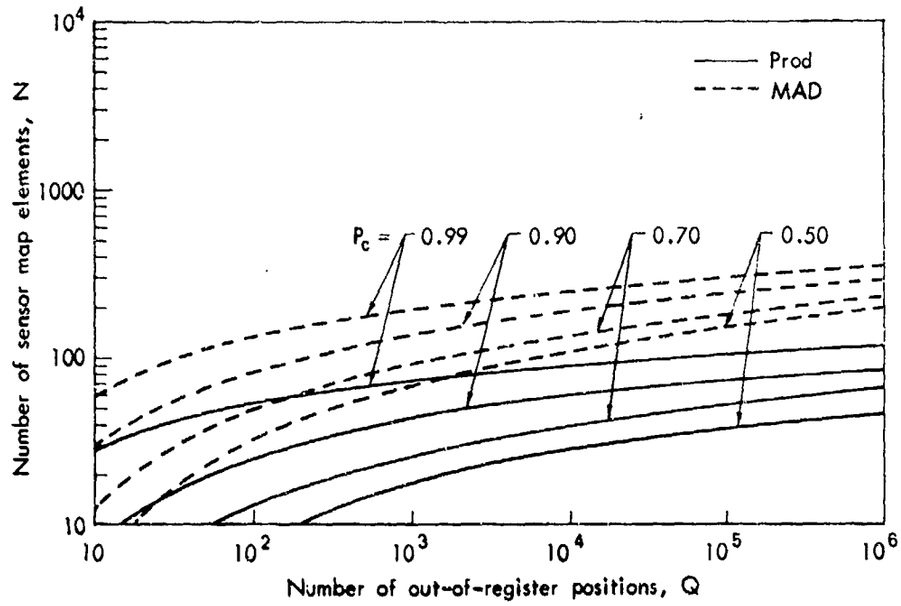

Fig. 11 — Probability contours for S/N = 30 + maximum synchronization error

for all S/N ratios (0.1 to 30) when worst-case synchronization errors are present. This result is easily understood if the lack of synchronization is interpreted (loosely) as an additional source of "noise," i.e., unavoidable differences between the two maps. Comparison of these results with Figs. 4 through 6, as illustrated explicitly in Fig. 12, shows that the effective value of S/N in the presence of worst-case synchronization errors is never greater than unity (on scenes with no spatial correlation); hence, according to the original finding with regard to S/N, the Product algorithm should be superior. Additional data on the relative degradation of P_c as a function of the magnitude and direction of the synchronization error is presented in Fig. 13 for a few specific situations.

MAGNIFICATION

With a magnification or scale factor error (assumed isotropic and constant over the map), as mentioned earlier, the sensor elements are dimensioned either somewhat larger or somewhat smaller than the reference map elements. The effects of such errors can again be analyzed by constructing an artificial reference map consisting of appropriately

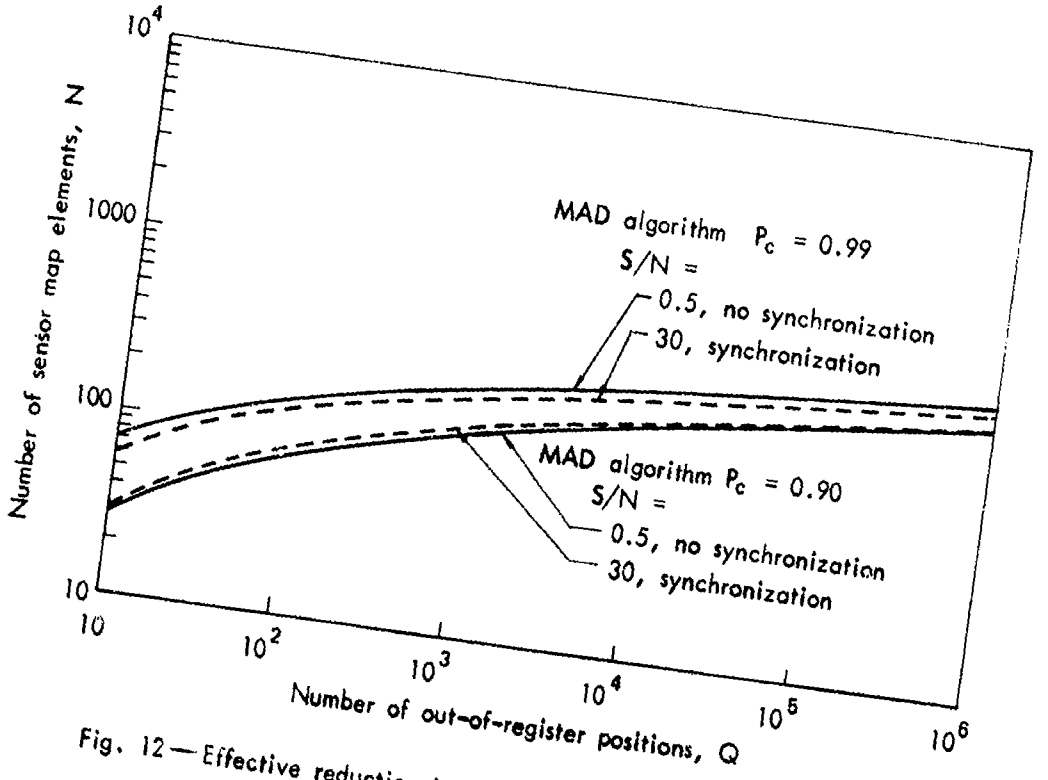

Fig. 12—Effective reduction in S/N ratio due to synchronization error using MAD algorithm

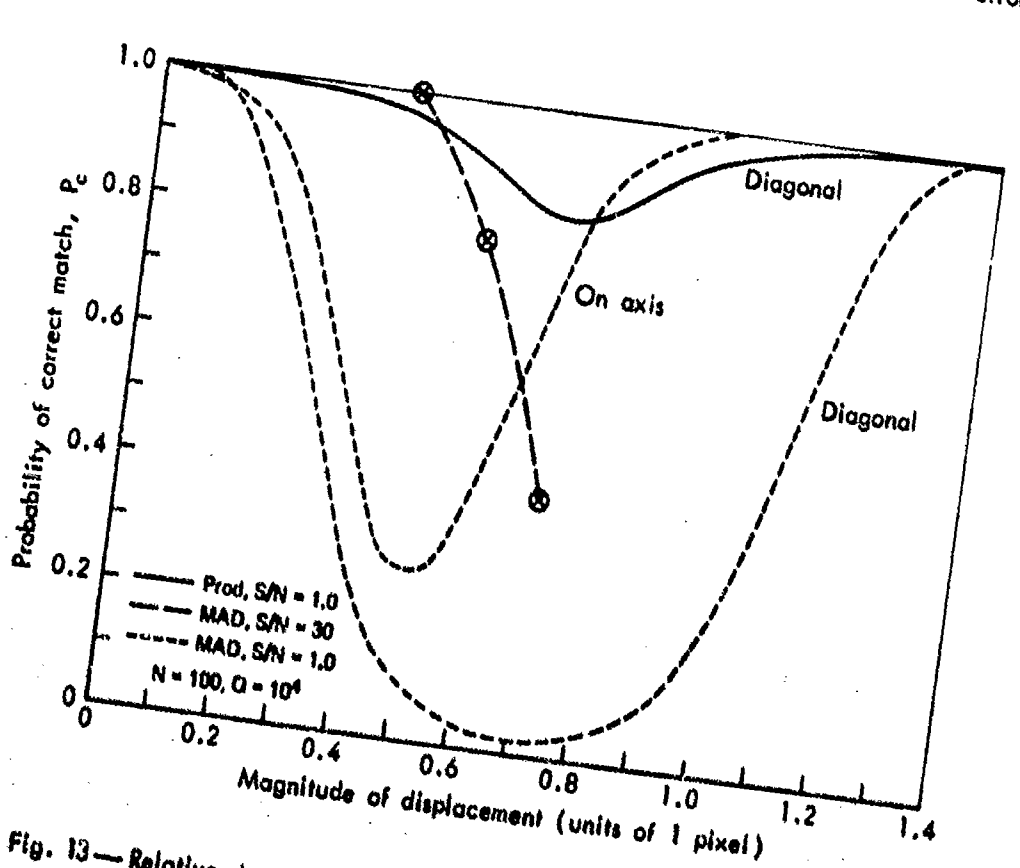

Fig. 13—Relative degradation in P_c versus magnitude of synchronization error

weighted combinations of the partially overlapping cells, and proceeding in a manner that is completely analogous to that used in analyzing synchronization errors. For the purpose of this analysis, the following values* of scale factor have been used:

$$\rho = 1.01,\ 1.02,\ 1.05,\ 1.1,\ 1.2,\ 1.5,\ 2\ ,$$

and the following sensor map sizes have been selected:

$$10 \times 10\ (N = 10^2)$$

$$30 \times 30\ (N = 9 \times 10^2)$$

$$100 \times 100\ (N = 10^4)$$

$$300 \times 300\ (N = 9 \times 10^4)$$

To illustrate how scale factor error both spreads the correlation function and decreases its peak value, consider a 10 × 10 sensor map and a function of the displacement that simply measures the total area of overlap obtained by summing over all cells. Table 1 shows this function for an array of displacements up to ±5 cells in both directions. When there is no scale factor error ($\rho = 1$) and the two maps are positioned on center, all 100 sensor map elements match their reference map counterparts. With each reference element defined to contain unit area, the match area in this case is 100 units, which produces (in the absence of noise or other errors) 100 percent overlap as shown. For any other displacement position, there is no match between reference and sensor elements and, as indicated in the table, the overlapping match area is zero.

As the scale factor is increased to 1.01, also shown in Table 1, the number of displacement positions for which there is at least partial overlap between the two maps increases from one to nine. In addition, the area of overlap at the center position has decreased from 100 units

*Values of $\rho < 1$ can best be treated by using the reciprocal values and interchanging the roles of reference and sensor maps.

Table 1

RELATIVE MAGNITUDE OF OVERLAP AREA WITH MAGNIFICATION ERRORS

(Map size: 10 × 10)

Scale Factor	Magnitude of Overlap Area										
	0.0	0.0	0.0	0.0	0.0	0.0	0.0	0.0	0.0	0.0	0.0
	0.0	0.0	0.0	0.0	0.0	0.0	0.0	0.0	0.0	0.0	0.0
	0.0	0.0	0.0	0.0	0.0	0.0	0.0	0.0	0.0	0.0	0.0
	0.0	0.0	0.0	0.0	0.0	0.0	0.0	0.0	0.0	0.0	0.0
	0.0	0.0	0.0	0.0	0.0	0.0	0.0	0.0	0.0	0.0	0.0
$\rho = 1$	0.0	0.0	0.0	0.0	0.0	100.00	0.0	0.0	0.0	0.0	0.0
	0.0	0.0	0.0	0.0	0.0	0.0	0.0	0.0	0.0	0.0	0.0
	0.0	0.0	0.0	0.0	0.0	0.0	0.0	0.0	0.0	0.0	0.0
	0.0	0.0	0.0	0.0	0.0	0.0	0.0	0.0	0.0	0.0	0.0
	0.0	0.0	0.0	0.0	0.0	0.0	0.0	0.0	0.0	0.0	0.0
	0.0	0.0	0.0	0.0	0.0	0.0	0.0	0.0	0.0	0.0	0.0
	0.0	0.0	0.0	0.0	0.0	0.0	0.0	0.0	0.0	0.0	0.0
	0.0	0.0	0.0	0.0	0.0	0.0	0.0	0.0	0.0	0.0	0.0
	0.0	0.0	0.0	0.0	0.0	0.0	0.0	0.0	0.0	0.0	0.0
	0.0	0.0	0.0	0.0	0.0	0.0	0.0	0.0	0.0	0.0	0.0
	0.0	0.0	0.0	0.0	0.02	1.47	0.02	0.0	0.0	0.0	0.0
$\rho = 1.01$	0.0	0.0	0.0	0.0	1.47	96.04	1.47	0.0	0.0	0.0	0.0
	0.0	0.0	0.0	0.0	0.02	1.47	0.02	0.0	0.0	0.0	0.0
	0.0	0.0	0.0	0.0	0.0	0.0	0.0	0.0	0.0	0.0	0.0
	0.0	0.0	0.0	0.0	0.0	0.0	0.0	0.0	0.0	0.0	0.0
	0.0	0.0	0.0	0.0	0.0	0.0	0.0	0.0	0.0	0.0	0.0
	0.0	0.0	0.0	0.0	0.0	0.0	0.0	0.0	0.0	0.0	0.0
	0.0	0.0	0.0	0.0	0.0	0.0	0.0	0.0	0.0	0.0	0.0
	0.0	0.0	0.0	0.0	0.0	0.0	0.0	0.0	0.0	0.0	0.0
	0.0	0.0	0.0	0.0	0.0	0.0	0.0	0.0	0.0	0.0	0.0
	0.0	0.0	0.0	0.0	0.0	0.0	0.0	0.0	0.0	0.0	0.0
	0.0	0.0	0.0	0.0	2.25	12.00	2.25	0.0	0.0	0.0	0.0
$\rho = 1.1$	0.0	0.0	0.0	0.0	12.00	64.00	12.00	0.0	0.0	0.0	0.0
	0.0	0.0	0.0	0.0	2.25	12.00	2.25	0.0	0.0	0.0	0.0
	0.0	0.0	0.0	0.0	0.0	0.0	0.0	0.0	0.0	0.0	0.0
	0.0	0.0	0.0	0.0	0.0	0.0	0.0	0.0	0.0	0.0	0.0
	0.0	0.0	0.0	0.0	0.0	0.0	0.0	0.0	0.0	0.0	0.0
	0.0	0.0	0.0	0.0	0.0	0.0	0.0	0.0	0.0	0.0	0.0
	0.0	0.0	0.0	0.0	0.0	0.0	0.0	0.0	0.0	0.0	0.0
	0.0	0.0	0.0	0.0	0.0	0.0	0.0	0.0	0.0	0.0	0.0
	0.0	0.0	0.25	1.25	1.50	1.50	1.50	1.25	0.25	0.0	0.0
	0.0	0.0	1.25	6.25	7.50	7.50	7.50	6.25	1.25	0.0	0.0
	0.0	0.0	1.50	7.50	9.00	9.00	9.00	7.50	1.50	0.0	0.0
$\rho = 1.5$	0.0	0.0	1.50	7.50	9.00	9.00	9.00	7.50	1.50	0.0	0.0
	0.0	0.0	1.50	7.50	9.00	9.00	9.00	7.50	1.50	0.0	0.0
	0.0	0.0	1.25	6.25	7.50	7.50	7.50	6.25	1.25	0.0	0.0
	0.0	0.0	0.25	1.25	1.50	1.50	1.50	1.25	0.25	0.0	0.0
	0.0	0.0	0.0	0.0	0.0	0.0	0.0	0.0	0.0	0.0	0.0
	0.0	0.0	0.0	0.0	0.0	0.0	0.0	0.0	0.0	0.0	0.0
	1.00	2.00	2.00	2.00	2.00	2.00	2.00	2.00	2.00	2.00	1.00
	2.00	4.00	4.00	4.00	4.00	4.00	4.00	4.00	4.00	4.00	2.00
	2.00	4.00	4.00	4.00	4.00	4.00	4.00	4.00	4.00	4.00	2.00
	2.00	4.00	4.00	4.00	4.00	4.00	4.00	4.00	4.00	4.00	2.00
	2.00	4.00	4.00	4.00	4.00	4.00	4.00	4.00	4.00	4.00	2.00
$\rho = 2$	2.00	4.00	4.00	4.00	4.00	4.00	4.00	4.00	4.00	4.00	2.00
	2.00	4.00	4.00	4.00	4.00	4.00	4.00	4.00	4.00	4.00	2.00
	2.00	4.00	4.00	4.00	4.00	4.00	4.00	4.00	4.00	4.00	2.00
	2.00	4.00	4.00	4.00	4.00	4.00	4.00	4.00	4.00	4.00	2.00
	2.00	4.00	4.00	4.00	4.00	4.00	4.00	4.00	4.00	4.00	2.00
	1.00	2.00	2.00	2.00	2.00	2.00	2.00	2.00	2.00	2.00	1.00

to approximately 96. The table shows a further decrease in the maximum overlap as ρ is increased to 1.1. When ρ is increased to 1.5, the number of displacement positions for which there is at least partial overlap between the two maps has increased to 49, and the maximum overlap has dropped to 9 percent of what it was when there was no scale factor error. Finally, when ρ = 2, the overlap function resembles a plateau covering the entire sensor map.

Table 2 conveniently summarizes the "width" of the overlap function in terms of the total number of displacement positions (including center) for which at least partial overlap exists as a function of the

Table 2

NUMBER OF OVERLAPPING POSITIONS AS A FUNCTION OF SCALE FACTOR AND MAP SIZE

Scale Factor, ρ	Overlapping Positions for Map Sizes of--			
	10 × 10	30 × 30	100 × 100	300 × 300
1	1	1	1	1
1.01	9	9	9	25
1.02	9	9	9	49
1.05	9	9	49	289
1.1	9	25	121	961
1.2	9	49	441	3,721
1.5	49	289	2,601	22,901
2.0	121	961	10,201	90,601

map size and scale factor. Table 3 summarizes the magnitude of the maximum value of the overlap function relative to the case with no scale factor error (ρ = 1), also as a function of map size and scale factor.

Tables 2 and 3 can be used as qualitative measures of how the scale factor degrades correlator performance. In order to keep the correlation width narrow (e.g., not more than nine cells) and the correlation peak relatively high (e.g., greater than 0.5), the relationships between map size and scale factor error given in Table 4 are

Table 3

RELATIVE MAGNITUDE OF THE CORRELATION FUNCTION PEAK AS A FUNCTION OF SCALE FACTOR ERROR AND MAP SIZE

Scale Factor, ρ	Magnitude of Correlation Peak for Map Sizes of--			
	10 × 10	30 × 30	100 × 100	300 × 300
1	1	1	1	1
1.01	.96	.86	.57	.11
1.02	.92	.74	.26	.03
1.05	.81	.42	.04	.005
1.1	.64	.13	.01	.001
1.2	.36	.04	.004	.0004
1.5	.09	.01	.0009	.0001
2.0	.04	.002	.0004	.00004

suggested as practical operating requirements. These relationships can be expressed by the following rule of thumb:

$$n(\rho - 1) \leq 1 \ , \tag{5}$$

which simply states that the displacement $(n/2)(\rho - 1)$ of a border cell should not exceed one-half cell width. Since maps as small as 10 × 10 will probably not be used in practice, this rule translates into a requirement on the scale (or on the estimated range to the target) of 1 to 5 percent--a not unreasonable requirement.

Table 4

APPROXIMATE RELATIONSHIPS FOR ALLOWABLE SCALE FACTOR ERROR AS A FUNCTION OF MAP SIZE

Map Size	Scale Factor
10 × 10	$\rho \leq 1.15$
30 × 30	$\rho \leq 1.04$
100 × 100	$\rho \leq 1.01$
300 × 300	Not to be used

The calculation of P_c in the presence of a scale factor error proceeds exactly as before. Results are presented in Fig. 14. It is apparent that scale factor errors always degrade correlator performance because of the decreased number of effectively matched cells.

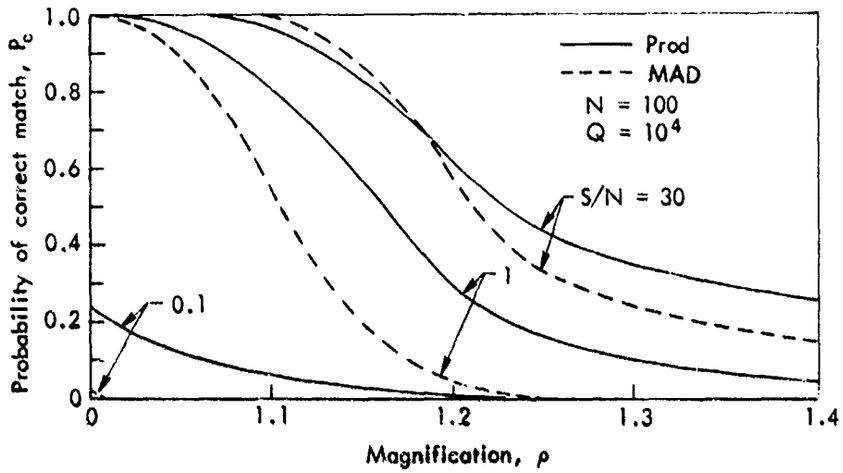

Fig. 14 — P_c as a function of magnification ρ

ROTATION

As with scale factor errors, a rotation between reference and sensor maps also increases the correlation spread over a larger number of displacement positions and decreases the peak of the correlation function. An illustrative example, similar to that provided for scale factor error, is shown in Table 5 for an assumed 10 × 10 sensor map. When there is no rotation error ($\theta = 0$) and when the map centers coincide, all 100 sensor map elements match their reference map counterparts; for any other displacement position, there is no overlap. As θ increases to 0.2 radian, as shown in Table 5, the nonzero overlap region spreads to nine cells and the magnitude of the maximum overlap decreases progressively. When θ reaches 0.5 radian, the number of displacement positions for which there is at least partial correlation between the two maps increases to forty-five.

A separate analysis, analogous to that used for scale factor errors, can be extended to determine P_c as a function of map size, rotation

Table 5

RELATIVE MAGNITUDE OF OVERLAP AREA WITH ROTATION ERRORS

(Map size: 10 × 10)

Rotation Error (radians)	Magnitude of Overlap Area										
	0.0	0.0	0.0	0.0	0.0	0.0	0.0	0.0	0.0	0.0	0.0
	0.0	0.0	0.0	0.0	0.0	0.0	0.0	0.0	0.0	0.0	0.0
	0.0	0.0	0.0	0.0	0.0	0.0	0.0	0.0	0.0	0.0	0.0
	0.0	0.0	0.0	0.0	0.0	0.0	0.0	0.0	0.0	0.0	0.0
	0.0	0.0	0.0	0.0	0.0	0.0	0.0	0.0	0.0	0.0	0.0
θ = 0	0.0	0.0	0.0	0.0	0.0	100.0	0.0	0.0	0.0	0.0	0.0
	0.0	0.0	0.0	0.0	0.0	0.0	0.0	0.0	0.0	0.0	0.0
	0.0	0.0	0.0	0.0	0.0	0.0	0.0	0.0	0.0	0.0	0.0
	0.0	0.0	0.0	0.0	0.0	0.0	0.0	0.0	0.0	0.0	0.0
	0.0	0.0	0.0	0.0	0.0	0.0	0.0	0.0	0.0	0.0	0.0
	0.0	0.0	0.0	0.0	0.0	0.0	0.0	0.0	0.0	0.0	0.0
	0.0	0.0	0.0	0.0	0.0	0.0	0.0	0.0	0.0	0.0	0.0
	0.0	0.0	0.0	0.0	0.0	0.0	0.0	0.0	0.0	0.0	0.0
	0.0	0.0	0.0	0.0	0.0	0.0	0.0	0.0	0.0	0.0	0.0
	0.0	0.0	0.0	0.0	0.0	0.0	0.0	0.0	0.0	0.0	0.0
	0.0	0.0	0.0	0.0	0.02	1.22	0.02	0.0	0.0	0.0	0.0
θ = .01	0.0	0.0	0.0	0.0	1.22	95.06	1.22	0.0	0.0	0.0	0.0
	0.0	0.0	0.0	0.0	0.01	1.22	0.02	0.0	0.0	0.0	0.0
	0.0	0.0	0.0	0.0	0.0	0.0	0.0	0.0	0.0	0.0	0.0
	0.0	0.0	0.0	0.0	0.0	0.0	0.0	0.0	0.0	0.0	0.0
	0.0	0.0	0.0	0.0	0.0	0.0	0.0	0.0	0.0	0.0	0.0
	0.0	0.0	0.0	0.0	0.0	0.0	0.0	0.0	0.0	0.0	0.0
	0.0	0.0	0.0	0.0	0.0	0.0	0.0	0.0	0.0	0.0	0.0
	0.0	0.0	0.0	0.0	0.0	0.0	0.0	0.0	0.0	0.0	0.0
	0.0	0.0	0.0	0.0	0.0	0.0	0.0	0.0	0.0	0.0	0.0
	0.0	0.0	0.0	0.0	0.37678	5.47182	0.37672	0.0	0.0	0.0	0.0
θ = .05	0.0	0.0	0.0	0.0	5.47200	76.60538	5.47161	0.0	0.0	0.0	0.0
	0.0	0.0	0.0	0.0	0.37663	5.47177	0.37676	0.0	0.0	0.0	0.0
	0.0	0.0	0.0	0.0	0.0	0.0	0.0	0.0	0.0	0.0	0.0
	0.0	0.0	0.0	0.0	0.0	0.0	0.0	0.0	0.0	0.0	0.0
	0.0	0.0	0.0	0.0	0.0	0.0	0.0	0.0	0.0	0.0	0.0
	0.0	0.0	0.0	0.0	0.0	0.0	0.0	0.0	0.0	0.0	0.0
	0.0	0.0	0.0	0.0	0.0	0.0	0.0	0.0	0.0	0.0	0.0
	0.0	0.0	0.0	0.0	0.0	0.0	0.0	0.0	0.0	0.0	0.0
	0.0	0.0	0.0	0.0	0.0	0.0	0.0	0.0	0.0	0.0	0.0
	0.0	0.0	0.0	0.0	0.0	0.0	0.0	0.0	0.0	0.0	0.0
	0.0	0.0	0.0	0.0	6.11771	12.58673	6.11764	0.0	0.0	0.0	0.0
θ = .2	0.0	0.0	0.0	0.0	12.58676	25.08639	12.58655	0.0	0.0	0.0	0.0
	0.0	0.0	0.0	0.0	6.11758	12.58671	6.11769	0.0	0.0	0.0	0.0
	0.0	0.0	0.0	0.0	0.0	0.0	0.0	0.0	0.0	0.0	0.0
	0.0	0.0	0.0	0.0	0.0	0.0	0.0	0.0	0.0	0.0	0.0
	0.0	0.0	0.0	0.0	0.0	0.0	0.0	0.0	0.0	0.0	0.0
	0.0	0.0	0.0	0.0	0.0	0.0	0.0	0.0	0.0	0.0	0.0
	0.0	0.0	0.0	0.0	0.0	0.0	0.0	0.0	0.0	0.0	0.0
	0.0	0.0	0.0	0.0	0.0	0.0	0.0	0.0	0.0	0.0	0.0
	0.0	0.0	0.0	0.001	0.146	0.618	1.286	0.694	0.0	0.0	0.0
	0.0	0.0	0.694	2.223	3.104	3.694	4.039	2.223	0.001	0.0	0.0
	0.0	0.0	1.286	4.039	4.103	4.068	4.103	3.104	0.146	0.0	0.0
θ = .5	0.0	0.0	0.618	3.694	4.068	4.098	4.068	3.694	0.618	0.0	0.0
	0.0	0.0	0.146	3.104	4.103	4.068	4.103	4.039	1.286	0.0	0.0
	0.0	0.0	0.001	2.223	4.039	3.694	3.104	2.223	0.694	0.0	0.0
	0.0	0.0	0.0	0.694	1.286	0.618	0.146	0.001	0.0	0.0	0.0
	0.0	0.0	0.0	0.0	0.0	0.0	0.0	0.0	0.0	0.0	0.0
	0.0	0.0	0.0	0.0	0.0	0.0	0.0	0.0	0.0	0.0	0.0

error, and search area. This tedious step can be avoided, however, if a relationship between scale factor errors and rotation errors can be found. Such a relationship seems intuitively plausible, at least for small rotation angles, and indeed one has been given by Lahart [6] as

$$\theta \approx \rho - 1 . \tag{6}$$

A comparison of the maximum area of overlap for scale factor and rotation errors is shown in Fig. 15 for the 10 × 10 (N = 100) map size. The agreement appears reasonably good, at least for the small rotation and scale factor errors that are of interest. A test of this relationship between θ and ρ was also made for the larger map sizes,

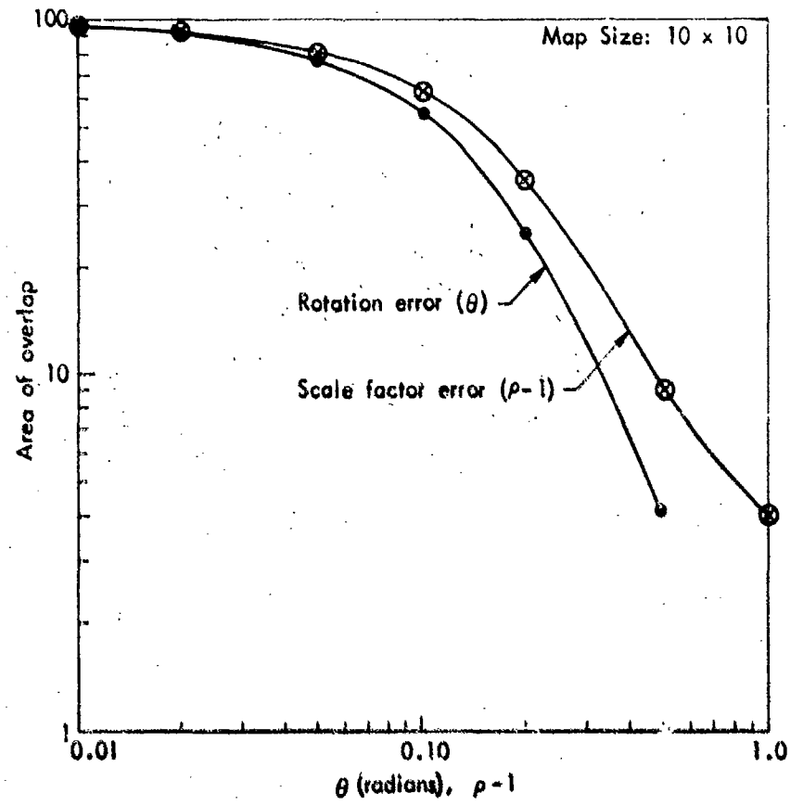

Fig. 15 — Comparison of the relative magnitude of the correlation peak for scale factor and rotation errors

and similar agreements were found.* To demonstrate real equivalence, it is also necessary to compare the relative shapes of the overlap functions for both error sources. This is done by comparing the overlapping match area at each displacement position, for two values of ρ and θ, with the sensor map containing 100 elements, as shown in Table 6. Considering the computational inaccuracies associated with determining the overlapping match area for both scale factor and rotation errors, the agreement is quite good.

Table 6

COMPARISON OF OVERLAP AREAS FOR SCALE FACTOR AND ROTATION ERRORS
(Map size = 10 × 10)

Scale Factor, ρ = 1.01	Rotation Errors, θ = .01	Scale Factor, ρ = 1.02	Rotation Errors, θ = .02
.02 1.5 .02 1.5 96. 1.5 .02 1.5 .02	.02 1.2 .02 1.2 95. 1.2 .02 1.2 .02	.09 2.9 .09 2.9 92. 2.9 .09 2.9 .09	.06 2.4 .06 2.4 90. 2.4 .06 2.4 .06

Consequently, on the basis of Lahart's analysis and the rough equivalence demonstrated here between scale factor error and rotation (for small rotation errors), the analysis of and pertinent conclusions about the effects of scale factor errors are carried over directly to the rotation problem. Specifically, the rule of thumb embodied in Eq. (5) is extended to

$$n\theta \leq 1 \tag{7}$$

in accordance with Lahart's formula given in Eq. (6). This corresponds to a rotation error (compass or attitude reference) of 1 to 5 percent of a radian or 0.6 deg to 2.9 deg (see Table 4)--again not an unreasonable requirement.

*A formula that is correct to 10 percent for $\rho < 1.4$ is $\theta = (\rho - 1)/[1 + 1.5(\rho - 1)]$.

ANALYSIS OF UNIFORM AMPLITUDE ERRORS

A qualitative discussion of the effects of systematic intensity errors has been given previously. The only case that has been analyzed quantitatively here is that of a uniform change in the overall signal level or gain by a factor K. The method is straightforward. Changes in the amplitude (or intensity) of the sensor scene relative to the reference scene do not affect the performance of the Product algorithm; but they can have drastic effects on the performance of the MAD algorithm, as illustrated in Fig. 16. The explanation of these results is straightforward. The Product algorithm attains its maximum whenever the sensor and reference map values are proportional to each other (see Part II of this study); therefore a change in the overall signal level by a constant factor has no effect. The MAD algorithm, on the other hand, attains its minimum value when the sensor and reference maps are *equal* to each other. Thus, the greater the change in the overall signal level, the more unequal are corresponding sensor and reference map values.

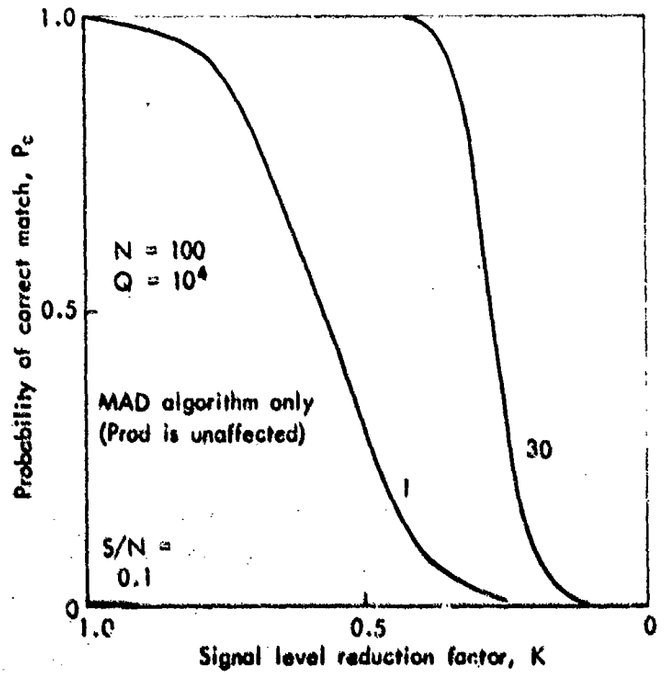

Fig. 16—Effect of signal level loss on P_c

CONCLUSIONS

In this section we have analyzed the effects of several commonly encountered error sources on two specific comparison metrics. Apart from the generation of certain constraints that must be satisfied if the effects of these errors are to be held within reasonable bounds, the most important conclusion to be drawn is the following: Real systems suffer from unavoidable synchronization errors, from geometrical distortions that can be partially controlled (at a cost) but not eliminated, and from amplitude changes some of which are partially controllable (such as quantization, discussed in Section IV, system malfunctions, and detector noise) but most of which are not controllable (the real changes in the scene). These systems are therefore invariably operated under conditions of rather low effective signal-to-noise ratios. Thus, despite the simplicity and the apparent advantages of a MAD algorithm or other differencing algorithms as presented in Section II, a Product algorithm will almost always be superior in real-world applications.

IV. SIMULATIONS USING REAL DATA

Inasmuch as real scenes exhibit various amounts of spatial correlation, and often quite non-Gaussian "structure" as well, it was important to test the theoretical conclusions presented in the previous sections using real-world data. This testing took the form of a number of computer simulations that are described in this section.

THE DATA BASE

The digitized imagery used for all the computer simulations described herein was taken from a computer tape obtained from Caltech's Jet Propulsion Laboratory (JPL) in Pasadena. This tape contains a digitized picture of a portion of Southern California, taken from an earth resources satellite in the near infrared band. The region is about 115 miles square, centered on the Antelope Valley; it includes the Los Angeles Basin and a significant length of coastline as prominent features. The original picture was about 2300 pixels (picture elements) × 3200 pixels, but was processed to yield a true (square) representation of 2300 × 2300 pixels. Each pixel represents a square area of about 80 m on a side, and takes on a gray-level value of 0 to 63.

The tape is especially interesting because it contains very different types of terrain and man-made features. Four distinctive square regions measuring 100 pixels (about 5 mi) on a side were selected for analysis. The four regions used are "agricultural," a part of the southern end of the San Joaquin Valley, characterized by fairly large and regular fields of various crops; "mountains," a distinctive mountainous area west of the desert; "desert," a relatively featureless and low-contrast area in the Mojave Desert; and "suburban," a portion of the San Fernando Valley in which there is a fairly regular grid of major roads.

One of the basic statistics of interest is the correlation length, because it effectively defines the size of a statistically independent scene element. Figure 17 shows the autocorrelation function, averaged

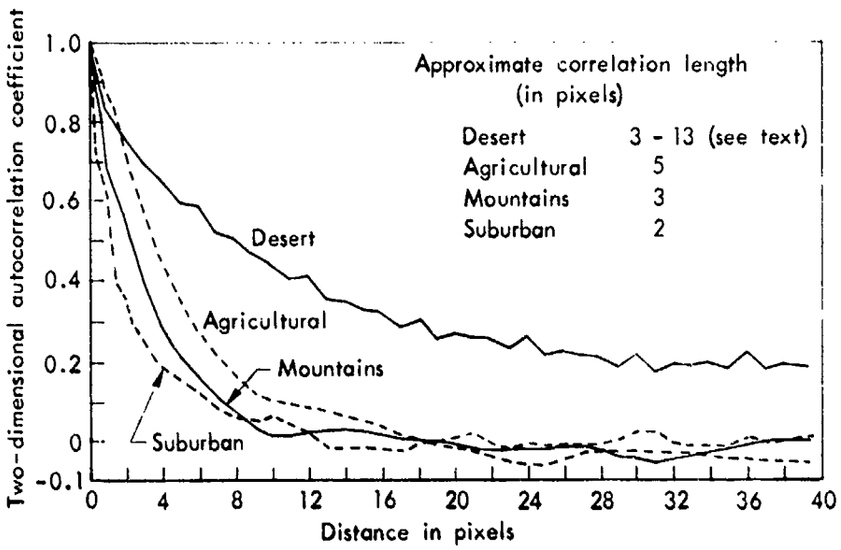

Fig. 17—Autocorrelation function for four selected scenes; each scene is 100 x 100 pixels (about 5 mi sq)

over both x- and y-directions, for each of the four regions. An effective "correlation length" can be defined in various ways. A common definition is the magnitude of the displacement for which the autocorrelation value is $1/e = 0.368$. Using this definition, the correlation lengths range from 2 for suburban to about 13 for desert.

The inadequacy of the concept of a single effective correlation length to characterize a real scene, and/or the inadequacy of the particular definition used here, is apparent from the graph. The desert autocorrelation coefficient initially falls off more sharply than that of the agricultural region, but then has a non-zero value for very large displacements and approaches zero very slowly. This phenomenon may be at least partially explained by the additional observation that, when the correlation length was calculated for various subregions, the value varied from about 3 to 13 for an average of about 8. Thus an accurate comparison with the previously obtained theoretical results is not to be expected in this case, since the effective number of statistically independent samples is poorly defined.

SIMULATIONS WITH NOISE ADDED

The most extensive simulations involved adding Gaussian noise to the sensor scene, and calculating the values of both the Product and the MAD metrics. The basic simulation paradigm used is as follows: Divide each 100 × 100-pixel region into twenty-five 20 × 20-pixel non-overlapping subregions; these are called the reference scenes. For each of these scenes, extract a smaller patch (generally 5 × 5 or 10 × 10) from the center, and call this the sensor scene. (Since the central 5 × 5 patch of a 20 × 20 subregion is not precisely defined, choose one of the four possible candidates arbitrarily and use it consistently thereafter.) Compute the mean and variance of each sensor scene and subtract the mean from each element so that the new mean is zero. Add Gaussian noise with zero mean and with a variance equal to some multiple of the observed sensor variance to obtain the desired S/N ratio. Superimpose this sensor scene on the reference scene in each of the possible displacement positions (16^2 positions for a 5 × 5, or 11^2 for a 10 × 10 sensor scene). For each superposition, also compute the mean of the portion of the reference scene with which it is to be matched, and remove its mean. Then apply each algorithm. If the extreme value of the metric occurs when the sensor scene (with noise) is placed in its original center position, then the search is a "success" on that 20 × 20 subregion. The number of successes over the 25 subregions for each algorithm can be computed and, in this manner, an empirical probability, P_c, thereby computed.

Simulations using the Product algorithm, i.e., the unnormalized product, resulted in a significant number of false matches. This, of course, is to be expected when relatively small-area scenes are compared, and even more so when the ensemble of scenes is not ergodic.*

*A specific numerical example will illustrate this problem. Consider the following "manufactured" 4 × 4 reference scene:

1	1	1	1
1	1	1	1
1	1	-3	-11
1	1	1	1

and define the 2 × 2 center block as the "sensor" scene. (Note that both the reference and sensor scenes have a zero mean.) If the Product

Hence the normalized Product algorithm (NProd), which is simply the classical correlation coefficient, was used in place of the Product algorithm.

Values of S/N = 1 and 3 were tried. At the higher value, almost perfect matches ($P_c \approx 1$) were obtained in all cases. The results for S/N = 1 are shown, together with the theoretical predictions for Gaussian ensembles, in Table 7. The empirical probabilities are, of course, each based on only 25 cases. The standard deviation of these values is given by $\sigma = [p(1 - p)/n]^{1/2}$, where p is the average value of P_c. Taking $p \approx 0.8$, it follows that $\sigma \approx 0.08$.

It is evident from these results that when real data are used, both algorithms perform significantly better, as measured by the fraction of correct acquisitions, than was predicted by the theory developed in Section II. The explanation probably lies in the fact that the statistics of real scenes are not Gaussian in nature, as was specifically assumed in the theory. That is to say, the specification of just two parameters--root-mean-square signal amplitude and a single correlation length--is far from adequate for characterizing terrain. It is obvious that two of the scenes, agricultural and suburban, contain structure (predominant spatial frequencies) that are, of course, far from Gaussian in character; however, careful tests or measurements of the degree of departure from Gaussian statistics have not been carried out. Nevertheless, the strong inference persists, supported by intuition, that correlation algorithms by their very nature are capable of exploiting these structural (non-Gaussian) features and thereby achieve high acquisition capabilities. A proper analysis of map-matching performance in the future can be expected to include not only the effects

---

metric is computed at each of the nine possible superposition locations, the maximum value will be found to occur at the right center position rather than at the true center, whether or not the mean of each 2 × 2 comparison area is subtracted out, because of the large contribution of the -11 (multiplied by -3) to the sum of products. If, on the other hand, the sum of products is normalized by dividing by the product of the standard deviations of the sensor scene and each 2 × 2 comparison scene of the reference map, any term containing the -11 will be reduced by the correspondingly larger standard deviation, with the result that the maximum value of the normalized Product metric occurs at the true center.

Table 7

COMPARISON OF THEORY WITH EXPERIMENT

(For ensemble of 25 scenes, S/N = 1)

Scene Type	Sensor Map Size (pixels)	Average Correlation Length (pixels)	Average Number of Independent Samples per Sensor Map, N	Average Number of Independent Comparisons, Q + 1	P_c (theory/experiment)	
					NProd	MAD
Agricultural	5 × 5	5	1	16	.22/.72	.06/.72
	10 × 10		4	9	.46/1.0	.34/1.0
Mountains	5 × 5	3	3	36	.24/.72	.05/.76
	10 × 10		11	19	.60/1.0	.41/1.0
Desert	5 × 5	11[a]	~ 1	6	.40/.92	.25/.92
	10 × 10		1	4	.46/1.0	.35/1.0
Suburban	5 × 5	2	6	72	.35/.92	.15/.80
	10 × 10		25	36	.82/1.0	.77/1.0

[a]This number is selected arbitrarily from those lying between the two values (8 and 13) cited in the text. It is emphasized again that no single number can be justified in this case.

of signal-to-noise ratio and spatial correlation (the Gaussian properties of a scene that have been considered in the foregoing), but also some yet-to-be-determined higher-order statistical parameters and/or special ad hoc feature descriptors.

One other experiment worth noting was conducted using this simulation technique. Since the expected value and variance of the in- and out-of-register correlation functions (as used in the P_c computation) are functions of the S/N ratio, it should be possible to estimate S/N from a set of observed expected values and variances. This could be of some interest because, in actual operations, an adaptive processing scheme might be used to select the best algorithm based on an initial estimate of the S/N ratio. This was tried for the MAD algorithm only. The procedure was (1) to compute from the data $\hat{\sigma}_R^2$, the variance of the reference scene that makes the MAD a minimum, (2) to use the square of the minimum correlation function value divided by $2/\pi^*$ for $\hat{\sigma}_N^2$, and (3) to take the ratio of $\hat{\sigma}_R^2/\hat{\sigma}_N^2$ as the S/N estimate. In fact, this procedure can be used if geometric distortions are also present. When the same expression* is used for the expected value of the in-register correlation function (because the proper expression for the S/N ratio with geometric distortion present is too complicated), the results show that one can estimate the equivalent S/N ratio from the data within about 10 percent of its actual value, even in the presence of added geometrical errors. This level of accuracy appears to be adequate for the kind of adaptive processor suggested at the beginning of this paragraph.

SIMULATION OF GEOMETRIC DISTORTIONS

Several of the errors treated analytically in Section III were subjected to a limited amount of simulation testing, using the real-world data described above. A program was written that introduces most of the several geometric distortions into the sensor map. The following limits were previously established for these error sources:

---

*$\bar{\phi}_o = (2/\pi)^{1/2}\,\sigma_n$ for the MAD algorithm (see second footnote, p. 10).

Synchronization ... Maximum ($\alpha_1 = \alpha_2 = \alpha_3 = \alpha_4 = 0.25$)
Scale factor ..... 10 percent ($\rho \leq 1.1$)
Rotation ..... 5.7 deg ($\theta \leq 0.1$)

All of these errors were added simultaneously, together with an S/N ratio of 3. The sensor map size chosen was 10 × 10 pixels (N = 100), a size that would be large enough to prevent anomalous results due to statistical fluctuations and at the same time would keep computer costs in check. The original 20 × 20 reference map size was retained. As before, an ensemble of twenty-five sensor maps for each scene type was compared with the corresponding reference maps, using both MAD and NProd algorithms. A correct lock-on was considered to be achieved if the extremum occurred in any one of the nine displacement positions (map center plus eight adjacent pixels) for which partial correlation was present.* This criterion was used because, as stated in Section I, this investigation is chiefly concerned with "false" acquisitions. It was assumed that different algorithms and appropriate interpolation routines could be employed to refine the accuracy of tracking after acquisition had been accomplished. The following results were obtained from this simulation:

P_c	Agricultural	Mountains	Desert	Suburban
For MAD	0.88	1.00	0.84	0.96
For NProd	0.96	1.00	0.96	1.00

These encouraging results are not unexpected, since in all cases the maximum linear displacement between cells is significantly less than a scene correlation length. In the worst case (smallest correlation length ≈ 2 for the suburban scenes), the assumed synchronization error corresponds to a 56 percent area overlap between independent scene elements. The maximum displacement at the edge of the sensor

*This number is correct when the scale factor or rotation error is taken alone; the correlation width when they are combined with a synchronization error is not known with certainty.

map, for the assumed scale factor plus rotation errors, produces the same displacement and degree of overlap; but in this case the average displacement over the sensor map is two-thirds of the maximum.

As shown in the above table, and as was predicted by the theory developed in Section II, these geometrical errors more severely degrade the MAD algorithm than they do the Product algorithm. However, it is clear that for this size reference and sensor map, geometric distortions at the levels investigated do not seriously degrade the acquisition capabilities of image correlators.

The theoretical analysis presented in Section III shows that, for the assumed error magnitudes, the probability of correct lock-on is close to unity for each type of geometric distortion taken separately in the presence of additive noise. These simulation results, with all error sources combined, are thus generally consistent with the theory. A further analysis to determine the combinations of distortion and map size for which significant degradation does occur was not made because geometric errors greater than those assumed here are considered unlikely in most operational situations.

SIMULATION OF INTENSITY CHANGES

The effects of systematic errors that result in changes in the amplitude of the sensor scene relative to the reference scene were also simulated. Both uniform intensity changes (e.g., a constant percentage reduction in all intensities) and environmental effects that cause block portions of the sensor scene to be completely different from their reference counterparts were tried.

UNIFORM GAIN CHANGES

The first experiment used the same maps with additive noise and with the same geometric errors (except 10 percent-of-maximum synchronization error) that were used in the geometric distortion evaluation. The amplitude of the sensor map was then reduced uniformly by factors of 0.75 and 0.50. The results of the computer simulations, based on twenty-five simulations per region, are shown in Table 8.

Table 8

EFFECT OF UNIFORM RELATIVE AMPLITUDE ERRORS
ON THE PROBABILITY OF CORRELATION

(S/N = 3)

	Relative Amplitude Factor					
	1.00		0.75		0.50	
Scene Type	MAD	NProd	MAD	NProd	MAD	NProd
Agricultural	0.96	0.96	1.00	1.00	0.56	0.92
Mountains	1.00	1.00	0.96	1.00	0.76	0.96
Desert	0.96	1.00	0.92	1.00	0.52	0.96
Suburban	1.00	1.00	1.00	1.00	0.64	1.00

In accordance with the Gaussian theory, the Product algorithm is not affected to any extent by uniform amplitude changes. The MAD algorithm, however, can be seriously degraded when intensity-scale changes occur, because the minimization of the metric requires an equality rather than merely a proportionality between the sensor and reference map values.

BLOCK SUBSTITUTIONS

Nonuniform amplitude errors that extend over groups of contiguous pixels are herein called block substitution errors. As discussed earlier, the presence of clouds or shadows or certain types of sensor malfunctions can cause errors of this type. A relatively crude experiment was conducted to test the effects of such block substitution errors. Central vertical strips of area 0.3, 0.5, and 0.7 of the whole sensor map were successively removed. Two different substitutions were made: in one the block was replaced by the mean value (zero), with no noise (possibly simulating a shadow); in the other the block was set equal to the maximum value occurring on the map, the new map was renormalized to zero mean, and then random noise was added to each pixel (thus simulating one possible form of jamming).

Table 9 shows the results of this experiment. As expected, degradation increases with increasing size of the substituted block, and

Table 9

EFFECT OF CERTAIN BLOCK SUBSTITUTION ERRORS ON THE PROBABILITY OF CORRELATION

(Noise added to sensor scene, S/N = 3)

	"Shadow" Effect						"Jamming" Effect					
	Fraction of Sensor Blocked Out--						Fraction of Sensor Blocked Out--					
	0.30		0.50		0.70		0.30		0.50		0.70	
Scene Type	MAD	NProd	MAD	NProd	MAD	NProd	MAD	NProd	MAD	NProd	MAD	NProd
Agricultural	1.00	1.00	.64	.84	.12	.56	.64	.68	.24	.36	.04	.04
Mountains	.96	1.00	.80	.84	.32	.68	.92	.88	.32	.28	.00	.08
Desert	1.00	1.00	.96	1.00	.36	.84	.80	.72	.32	.40	.00	.24
Suburban	1.00	1.00	.76	.96	.48	.68	.64	.52	.20	.36	.00	.08

depends somewhat on the scene type. Less degradation occurs when the block is set equal to the mean value of the sensor map than when it is set to the maximum value. It also appears that the Product algorithm is much more resistant to large-block substitution errors than is the MAD algorithm, particularly in the case of "shadows"; but both are seriously degraded in the presence of high-intensity jamming.

Of course, the above conclusions apply only to the particular types of block errors considered. Many more simulation runs would have to be made with other types of errors in order to provide general validation of these findings. Nevertheless, the results are quite interesting, and confirm what intuition would dictate. They also suggest directions for future research.

GRAY-LEVEL QUANTIZATION

The effects of gray-level quantization have been explored briefly in two experiments, using a few simple encoding schemes. Quantization necessarily introduces some degradation of the map-matching process because information is always lost; thus, with binary coding, every gray level is recorded as either -1 or 1--a drastic level of data compression and information loss. On the other hand, computations can be greatly simplified if the data levels can be reduced to a small number.

In the first experiment, a completely random and uncorrelated 20 × 20-pixel map was generated with continuous (6-digit Gaussian random number) gray levels. The central 5 × 5 and 10 × 10 portions were extracted, to which noise with the same standard deviation (S/N = 1) was added 100 different times. Then the intensity levels in each cell of both maps were quantized into each of the three coding schemes shown in Table 10, and correlations were carried out using both

Table 10

QUANTIZATION CODES

True level	$-\infty$	-1.5σ	-1.0σ	-0.5σ	0	$+0.5\sigma$	$+1\sigma$	$+1.5\sigma$	∞
Two-level code	-1					+1			
Four-level code	-2		-1			+1		+2	
Eight-level code	-4	-3	-2	-1		+1	+2	+3	+4

MAD and Product algorithms. It was found that with the 10 × 10 maps, P_c was essentially equal to unity for these quantization schemes. Using the 5 × 5 maps, the results given in the first row of Table 11 were obtained.

These results show that P_c increases monotonically (as expected) with the number of quantization levels and that 8-level (i.e., 3-bit) quantization schemes yield results close to the continuous case. There are two additional points worth noting. First, when the data are quantized, there is a finite possibility that the correlation function will take on its extremum value at several displacement positions. Whenever this occurred in the simulations, it was counted (conservatively) as a false lock, even though the true center was among the displacement positions that produced the extremum. Second, it is observed that the MAD and Product algorithms are identical for binary coding schemes. This fact can be demonstrated in general by means of a truth table for the product and for $1 - |\text{diff}|$.*

*This equivalence was first pointed out to the authors by R. L. Sendall of Hughes Aircraft Company.

Table 11

EXPERIMENTAL VERIFICATION OF EFFECT OF QUANTIZATION ON THE PROBABILITY OF CORRELATION

(N = 25, S/N = 1)

	Quantization Scheme							
	Continuous		8-level		4-level		Binary	
Scene Type	MAD	NProd	MAD	NProd	MAD	NProd	MAD	NProd
Random	.90	.95	.78	.87	.65	.74	.30	.30
Agricultural	.72	.72	.64	.52	.36	.40	.36	.36
Mountains	.76	.72	.60	.60	.36	.32	.28	.28
Desert	.92	.92	.80	.80	.48	.56	.36	.36
Suburban	.80	.92	.72	.80	.68	.72	.36	.36

In the second experiment, the same quantization schemes were applied to the usual JPL digitized scenes. The S/N ratio was set at 1, and a 20 × 20 reference map and a 5 × 5 sensor map were used. The results are given in Table 11, together with the results for the random scene. In this table, "continuous" denotes use of the original data with no modification. It should be remembered, however, that the original data itself is quantized to 64 levels, and that in practice somewhat fewer levels are generally present in any region because of a certain homogeneity within the region (especially in the desert). With the exception of the binary case, these data show that the real (partially correlated) scenes yield lower values of P_c than the artificial random scene; this conforms with the Gaussian theory, since, for the same number of pixels, there are fewer independent data samples in the real scenes.

The same two conclusions regarding the number of quantization levels hold in this case as for the artificial map. Thus 8-level quantization (or possibly 16-level in some cases) is expected to be sufficient for practical system applications. It should also be noted that a number of other coding schemes--altering the values assigned to each level and the demarcations between levels--should be investigated until nearly optimum codes are demonstrated.

LOCAL OPERATORS

Finally, some very preliminary experiments using local operators to preprocess the imagery were undertaken. The purpose of these experiments was to determine whether the probability of correct acquisitions could be improved when such operators are used. Much research has been done elsewhere on such techniques as contrast enhancement and edge detection, and their application to real-world imagery has yielded spectacular results in some cases, e.g., the visual enhancement of pictures returned from the moon and minor planets. The application of such techniques to image correlation involves the preprocessing of both reference and sensor scenes in a manner that will enhance those features contributing most strongly to a successful correlation while suppressing the noise.

Operators are generally of two types, global or local. "Global" refers to operators that transform the picture as a whole, such as histogram equalization or Fourier transformation. Local operators transform a small portion of the picture at a time, but are generally applied repetitively over the whole picture. Our experiments to date have been limited to local operators.

Two simple local operators were applied to each scene through computer simulation programs similar to those described previously. The values of N, Q, and S/N were the same as those used in the earlier simulations, so the results can be directly compared.

The first local operator applied is referred to as a Laplacian, because it is one of a class of operators used to form a finite-difference approximation to the continuous Laplacian operator (sum of second partial derivatives). The particular one employed here is the following two-dimensional weighting function:*

$$\begin{matrix} -1 & -1 & -1 \\ -1 & 8 & -1 \\ -1 & -1 & -1 \end{matrix}$$

*The factor 8 is provided only to preserve a zero mean. When applied to an edge or corner of the map, the weighting function is appropriately truncated and the central factor is modified accordingly.

In use, this function is convolved with every point of the picture. Thus the value of the map at a given point is replaced by the weighted sum of products of map and weighting function values over a neighborhood of 9 pixels.

The simulation was done exactly like the additive noise simulation described earlier, except that 7 × 7 patches were extracted from the original map (before application of the Laplacian) to form the sensor scene. Gaussian noise (S/N = 1) was then added to the 7 × 7 map and the Laplacian was applied to this noisy map. In this case the edges were later discarded, leaving a 5 × 5 sensor map. (It is usually not necessary to subtract the means, because the Laplacian operator generally produces a mean that is small in relation to the standard deviation.) Both the NProd and MAD algorithms were applied and "successes" were recorded if the extremum occurred when the two map centers coincided. The empirical probabilities thus determined are shown below:

P_c	Agricultural	Mountains	Desert	Suburban	Theory
For MAD	.40	.24	.60	.48	.50
For NProd	.40	.28	.76	.56	.70

These results are more nearly in agreement with the original theoretical predictions of Section II (S/N = 1, N = 25, Q = 255) than were those for the unprocessed scenes, a situation that may possibly be explained by the fact that the application of the Laplacian operator tends to produce pictures with statistics that are more nearly Gaussian. However, it is noteworthy that the application of the Laplacian does not result in greater improvement, possibly because the Laplacian, being basically a point operator, tends to emphasize isolated noisy points. It is speculated that some smoothing of the data and/or application of a larger Laplacian (say, 9 × 9 in place of 3 × 3), would alleviate this problem; however such experiments have not been attempted as of this writing.

The second local operator tried was a type of scalar gradient. A true (vector) gradient is somewhat difficult to handle and is presumably sensitive to rotation errors. The scalar gradient used was the average magnitude of the change in gray-scale value between a pixel and its 8 neighbors. This gradient is not unlike several that have appeared in the literature and is somewhat like an edge-detection operator.

By using this gradient, and applying the same general procedure as with the Laplacian but with the mean subtracted, we obtained the following results for the probability of correct acquisition:

P_c	Agricultural	Mountains	Desert	Suburban	Theory
For MAD	.16	.08	.16	.12	0.50
For NProd	.04	.00	.16	.16	0.70

These first results are quite poor and indicate that at least this version of the gradient is not very useful. The effort on preprocessing, using various local operators, is continuing.

CONCLUSIONS

There are two conclusions to be drawn from the real-world-scene experimental work that has been described in this section. The first, and quite significant, conclusion is that correlation devices generally perform better on real scenes than is predicted by simple Gaussian theory. The second conclusion is that the predicted effects of various geometrical distortions and of changes in signal amplitudes, including quantization effects, are generally confirmed. Some very preliminary attempts to use preprocessing "filters" are still quite inconclusive.

V. MAJOR CONCLUSIONS AND FUTURE PLANS

The principal, overall conclusion of this study is that an approximate lower bound on the value of P_c--the probability of correct (and autonomous) target acquisition--can be calculated, so that one can, at least in principle, design systems to meet an acquisition specification.

Quantitative relationships have been presented that show the dependence of P_c on N (the sensor map size), M (the search area or reference map size), S/N (nominally the signal-to-noise ratio but, more importantly, a measure of the fidelity of the reference map vis à vis the real-time sensor map), and various parameters describing systematic intensity and geometrical errors. Thus one has the tools for carrying out design tradeoffs on sensor resolution and field of view (to increase N), on midcourse navigation (to decrease M), on attitude reference and guidance (to reduce geometrical distortions), on data processing capabilities (to reduce both synchronization and quantization effects), on more recent and more accurate reference data (to increase S/N), and so on, including, finally, a tradeoff of the cost of increasing the P_c requirement itself with the loss of those few weapons that will be wasted if they achieve a false lock.

Most of the above-mentioned relationships for P_c are derived from a simple Gaussian theory that is known to be unrealistic. Fortunately, however, this theory appears to err on the conservative side--most scenes are more distinctive than assumed and results are better than predicted. On the other hand, real systems have additional error sources that have not been analyzed in the experiments conducted in this study. The important point is that, with a "floor" established for P_c, there should be no major surprises in future flight tests of either experimental or operational hardware in the field of image correlation guidance; improvements in the theory, and additional data from simulation experiments using specific scenes of interest, can only improve the predictions and relax some of the design restrictions. One *can* design to P_c requirements, though at the moment not as effectively as would be desired.

The second major conclusion of this study is that one *may* find better algorithms in the future than those that have usually been used in the past. The argument runs as follows: It is shown in Part II of this study that, in general, there is not a unique or demonstrably optimum algorithm for maximizing the acquisition capability of a map-matching or image correlation guidance system. This statement is a consequence of the fundamental nature of the map-matching process, which involves, in any real situation, the comparison of nonidentical imagery. Furthermore, simulation experiments are reported in Section IV in which the acquisition probabilities obtained by using real scenes were higher than those predicted by straightforward Gaussian theory. It was concluded that this phenomenon is due precisely to the special features--i.e., the non-Gaussian structure--that are present in most scenes and that render them more distinctive than samples of pure Gaussian noise would be.

Based on these two conclusions, the authors believe that approaches founded on feature selection may lead to more efficient methods for implementing this class of guidance system. Rather than to simply refine algorithms that still compare every pixel in the sensor and reference scenes, one should search for powerful preprocessing schemes to extract the "most unique" features. One would perhaps apply several feature-selecting algorithms to a reference scene until "good" or efficient features were found for each specific scene; then not only would the reference map be modified, but the on-board preprocessor would be instructed to look for the same chosen features in the sensor map. As a consequence, the chances for a false lock should be reduced, and at the same time the amount of real-time processing required should also be reduced. The degree of improvement cannot be known at the present time; for some scenes it will be negligible, but for others it may be substantial. Only further study and experimentation can resolve this point. Since the expected operational context involves getting prior imagery anyway, this concept may be quite appropriate for military applications.

Instead of using conventional feature-extraction algorithms, current plans are to develop procedures that relate more closely to the problem at hand. For example, one need only determine where map A falls

within map B; it is not necessary to assign a classification to map A according to standard pattern recognition methods. Although these procedures can provide some guidance, certain new techniques seem more promising, particularly the extraction of features that seem visually unique, such as road intersections and certain other man-made objects that lend "distinctiveness" to a picture. This idea may be generalized and a form of local pseudoentropy may be calculated as a device for isolating such features. Furthermore, the relationships of these features to each other can provide valuable cues. Syntactic pattern recognition, which takes such relationships into account, can be a useful tool here; however, care must be taken to use just that which is appropriate, without an overemphasis on formalism. Some techniques from the field of artificial intelligence may also be employed.

Rand does not claim to be the first to arrive at this point of view. We have, however, reached it completely independently and by a route that was somewhat surprising to us. We have also tried to document the rationale for this point of view better than it has been documented elsewhere. Although of course not alone, we hope to pursue this new approach in some detail during the coming months.

PRECEDING PAGE BLANK-NOT FILMED

REFERENCES

1. Wessely, H. W., *Image Correlation, Part II: Theoretical Basis*, The Rand Corporation, R-2057/2-PR, November 1976.

2. Bailey, H. H. *A Fundamental Approach to "Map-Matching" Area Correlators*, The Rand Corporation, RM-5308-PR, April 1967.

3. *TERCOM False Fix Study* (U), ASD-TR-72-74, E-Systems, Inc. (Garland Division), September 1972 (Secret).

4. Carpenter, T. A., J. M. Dodd, and J. K. Matsunaga, *Design Study of Radiometric Area Correlation Guidance* (U), AFAL-TR-71-242, Lockheed Missiles and Space Company, Inc., April 1972 (Secret). (See especially Vol. 2, p. 47.)

5. Johnson, M. W., *Analytical Development and Test Results Used in Navigation Systems*, AIAA Paper 72-122, presented at the Tenth Aerospace Sciences Meeting (San Diego), January 1972.

6. Lahart, M. J., "Optical Area Correlation with Magnification and Rotation," *J. Opt. Soc. Amer.*, Vol. 60, No. 3, March 1970, pp. 319-325.

UNCLASSIFIED

SECURITY CLASSIFICATION OF THIS PAGE (When Date Entered)

REPORT DOCUMENTATION PAGE

READ INSTRUCTIONS BEFORE COMPLETING FORM

1. REPORT NUMBER: R-2057/1-PR	2. GOVT ACCESSION NO.
3. RECIPIENT'S CATALOG NUMBER	
4. TITLE (and Subtitle): Image Correlation: Part I. Simulation and Analysis.	5. TYPE OF REPORT & PERIOD COVERED: Interim rept.
	6. PERFORMING ORG. REPORT NUMBER
7. AUTHOR(s): H. H. Bailey, E. W. Blackwell, C. L. Lowery, J. A. Ratkovic	8. CONTRACT OR GRANT NUMBER(s): F44620-73-C-0011
9. PERFORMING ORGANIZATION NAME AND ADDRESS: The Rand Corporation, 1700 Main Street, Santa Monica, Ca. 90406	10. PROGRAM ELEMENT, PROJECT, TASK AREA & WORK UNIT NUMBERS
11. CONTROLLING OFFICE NAME AND ADDRESS: Project AIR FORCE Office (AF/RDQA), Directorate of Operational Requirements, Hq USAF, Washington, D.C. 20330	12. REPORT DATE: November 1976
	13. NUMBER OF PAGES: 53
14. MONITORING AGENCY NAME & ADDRESS (if different from Controlling Office): 64p.	15. SECURITY CLASS. (of this report): UNCLASSIFIED
	15a. DECLASSIFICATION/DOWNGRADING SCHEDULE

16. DISTRIBUTION STATEMENT (of this Report)

Approved for Public Release; Distribution Unlimited

17. DISTRIBUTION STATEMENT (of the abstract entered in Block 20, if different from Report)

No restrictions

18. SUPPLEMENTARY NOTES

19. KEY WORDS (Continue on reverse side if necessary and identify by block number)

Images
Maps
Target Discrimination
Optical Tracking
Pattern Recognition
terminal guidance

20. ABSTRACT (Continue on reverse side if necessary and identify by block number)

see reverse side

DD FORM 1 JAN 73 1473 EDITION OF 1 NOV 65 IS OBSOLETE

296 600

UNCLASSIFIED

SECURITY CLASSIFICATION OF THIS PAGE (When Date Entered)

Investigates image correlation for map matching in target acquisition and tracking both theoretically and by using computer simulations. The emphasis is on the acquisition phase, particularly (a) the probability of achieving a correct match, (b) selection of an appropriate comparison metric to maximize this probability. Study conclusions: Using methods outlined in this report, an approximate lower bound on the value of the probability of a correct match can be calculated. Several quantitative relationships between this probability and various system parameters have been derived and largely confirmed by simulation testing. The second conclusion is that there ought to be better algorithms than those used in the past. It is reasonable and consistent with theory to search for more efficient ways to carry out the initial map-matching or target-acquisition function. Preprocessing to extract special features using techniques of pattern recognition appear promising for the generation of more efficient algorithms. Future research in this area is outlined. Ref. (AR)